공학박사학위논문

Engineering the Deformation Characteristics of Soft Materials through Geometric Design of Auxetics for Flexible Electronics Application

옥세틱 구조개발을 통한 소프트 재료의 변형 특성 설계 및 유연소자 적용에 대한 연구

2017년 8월

서울대학교 대학원

재료공학부

이 영 주

옥세틱 구조개발을 통한 소프트 재료의 변형특성 설계 및 유연소자 적용에 대한 연구

ENGINEERING THE DEFORMATION CHARACTERISTICS OF SOFT MATERIALS THROUGH GEOMETRIC DESIGN OF AUXETICS FOR FLEXIBLE ELECTRONICS APPLICATION

지도교수: 주 영 창

이 논문을 공학박사 학위논문으로 제출함

2017년 8월

서울대학교 대학원

재료공학부

이 영 주

이 영 주의 박사학위 논문을 인준함

2017년 7월

위 원 장	선 정 윤	(인)
부 위 원 장	주 영 창	(인)
위 원	조 규 진	(인)
위 원	최 인 석	(인)
위 원	채 경 훈	(인)

ABSTRACT

Engineering the Deformation Characteristics of Soft Materials through Geometric Design of Auxetics for Flexible Electronics

As the development of flexible devices has progressed for user's convenience, researches on the rational design of architectures and structures which could provide mechanical functionality to flexible devices, have been actively carried out as well as material development perspective. The control of mechanical properties through structural innovation has the advantage that it provides unprecedented properties beyond the existing material limits and is easy to design predictably. Based on this feature, there is a growing interest in reconfigurable materials that could operate in response to external physical stimuli. Auxetics, which are one of the mechanically reconfigurable materials, is a structure which are able to perform negative Poisson's ratio behavior. Based on the characteristics, auxetics have an excellent expandability and possible to maintain an excellent conformability even on a non-zero Gaussian surface. Therefore, auxetics are an attracting attention as a structural material for a next generation flexible device. In this thesis, the mechanical and electrical performance of flexible devices were improved through proper geometric design of two dimensional auxetic structure, and suggested auxetics as a new paradigm of structural materials for flexible devices.

At first, a platform for flexible devices was proposed, which was capable of large displacement in all directions by using a rotational unit auxetic including a self-similar hierarchical structure. Through the finite element analysis, it was proved that even if the hierarchical auxetic was subjected to complicated deformation, not only the tension but

also crumpling, the deformation could be concentrated only in the hinges connecting the individual unit. Based on the deformation characteristics, an omnidirectionally and extremely deformable battery was developed. When the hinge was composed of an elastomer having excellent mechanical reliability, it was possible to deform the hinge in an unexpected three dimensional manner beyond the viewpoint of the conventional two dimensional auxetic view. As a result, the degree of freedom of hinge deformation could be increased to infinity. Also, as the level of the hierarchical structure increased, the strain concentrated on the hinge is relaxed even at the same level of strain, thereby improving the mechanical stability and improving the stretchability and be crumpled easily. In addition, it was possible to design the same hierarchical auxetic in a thin plastic substrate through the cutting process. In this case, the sharp cut pattern could cause tearing, which could result in severe mechanical failure. To improve the mechanical reliability at the hinge, a design to prevent the crack propagation was proposed, thereby confirmed the potential ability of applying the hierarchical auxetic to thin sheets.

Secondly, a hybrid auxetic composite had been developed which could be predictably design the modulus of elasticity and Poisson's ratio, by embedding two dimensional re-entrant auxetic as a composite scaffold into soft material. This composite could have an anisotropic deformation behavior due to the influence of re-entrant structure, which had a negative Poisson's ratio behavior in in-plane and a positive Poisson's ratio in the normal direction. Especially, the thickness of matrix in the composite could be decreased even more compared to the conventional isotropic materials due to the volume conservation. Using the anisotropic mechanical property of composite, a stretchable capacitive strain sensor having improved sensing property was developed which could stretch up to 50 %. The Gauge factor, which is a ratio of change in capacitance to the stretch, of the conventional capacitive strain sensor was limited to

1 due to the geometric factor. Applying the auxetic composite as a dielectric, sharper capacitance change was achieved even under the same degree of stretch compared to the conventional sensor. In addition to the improvement, the composites could represent a good conformability to such as elbows and knees, thus our composites could suggest a new direction in geometry design for wearable sensors.

This thesis suggested auxetics as a new paradigm as a structural material for flexible devices by improving the mechanical and electrical performance of various flexible devices that are currently being developed, by properly customizing the architectural design.

Young-Joo Lee

Department of Materials Science and Engineering

The Graduate School

Seoul National University

Keywords: Auxetic, Geometric engineering, Reconfigurable materials, Flexible electronics, Mechanical metamaterial

***Student Number*:** 2011-20659

Table of Contents

LIST OF TABLES

LIST OF FIGURES

CHAPTER 1

Introduction

1.1 Emergence of soft electronics

Recent electronic devices have evolved to be bendable, twistable, and stretchable without any mechanical failure. Soft electronics, which means that the device could be deformable, included all kinds of devices that could be deformable. The early stages of soft electronics were the devices positioned on the thin substrate such as a polymeric or metal foil substrates, which could be easily bent. However, these kinds of electronics cannot be stretched or deformed severely. From this reason, researches of soft material based electronics were bending investigated intensively in these days.

Soft materials, which was normally accepted as easily deformable materials (Young's modulus usually less than 10^2 MPa), include liquids, gels, polymers, foams, etc. Due to the physical property, soft material based electronic devices could undergo severe mechanical deformation without any kinds of mechanical breakdown. To fabricate the

electrical performance, soft materials have been developed to contain electrical properties such as combining metallic composites, ionic gels, liquid metals, and even could be used as epidermal electronics if the biocompatibility of materials could be satisfied. Based on the aforementioned characteristics, the soft electronics are the promising future technologies which could be applied to the electronic skin, soft robots, wearable and epidermal sensors and actuators.[1-4] **Figure 1.1** is the historical map of evolution in soft electronic devices.

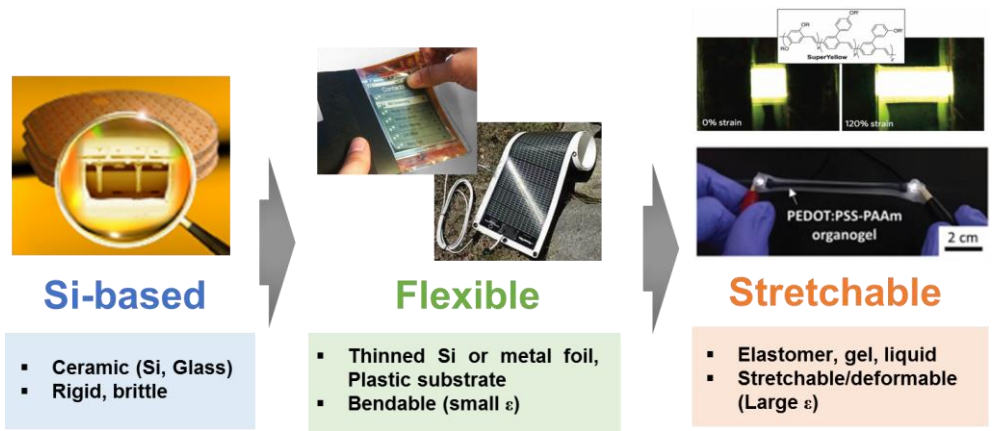

Figure 1.1 Evolution of soft electronics. The material elements were getting softer as the device evolved.

1.2 Necessity of geometric design for soft electronics

Present studies of developing soft electronics have been mainly performed to develop soft materials that could contain electrical functionality. Because soft materials had low Young's modulus and higher yield strain where the irreversible deformation compared to conventional electronic materials, application to flexible devices through the development of soft materials may be quite natural.

In addition to the development of material, there is another strategy to fabricate soft electronics: a structural aspect. Recently, researches focused on the 'flexible structure' have been gradually increasing in addition to the development of soft materials to realize the flexible electronics.[5-9] Designing the flexible structures mean that the structures could relieve or avoid mechanical stress which evolved from the external force, thereby preventing the failure of materials even under the large deformation condition. Such an improvement based on the structural perspective had advantages that the high-performance material which has been used in the conventional electronic device can be used without consideration of compatibility problem.

Especially, the strategy that controlling the mechanical properties of materials through structural design is most prominent because it could have mechanical characteristics that cannot be possessed by conventional materials in terms of macroscopic departure from the limit of material synthesis. Structural engineering, which controlled the mechanical properties of materials through consideration of geometric factors, was also a more advantageous aspect than material synthesis in that the global mechanical property could be predictably designed.

On the basis of these characteristics, there has been a lot of researches on structural design for relieving or avoiding mechanical stress by imparting flexibility or specific shape programming recently. In particular, reconfigurable materials whose shape could change through external stimuli such as electricity, magnetism, heat, and force have been attracting great attention due to their various potential applications. These reconfigurable materials were able to characterize not only by the influence of external stimuli but also by the physical factors depending on the geometrical factors, so that appropriate structural design was required according to the desired application.

In this thesis, improving the electrical and mechanical performance characteristics of flexible devices were achieved through the proper geometric design of mechanically reconfigurable materials. The research contained stress/strain analysis according to mechanical deformation through finite element method and suggested practical applications to electronics. In this study, we use a structural metamaterial called 'Auxetic' as a key structure for flexible devices.

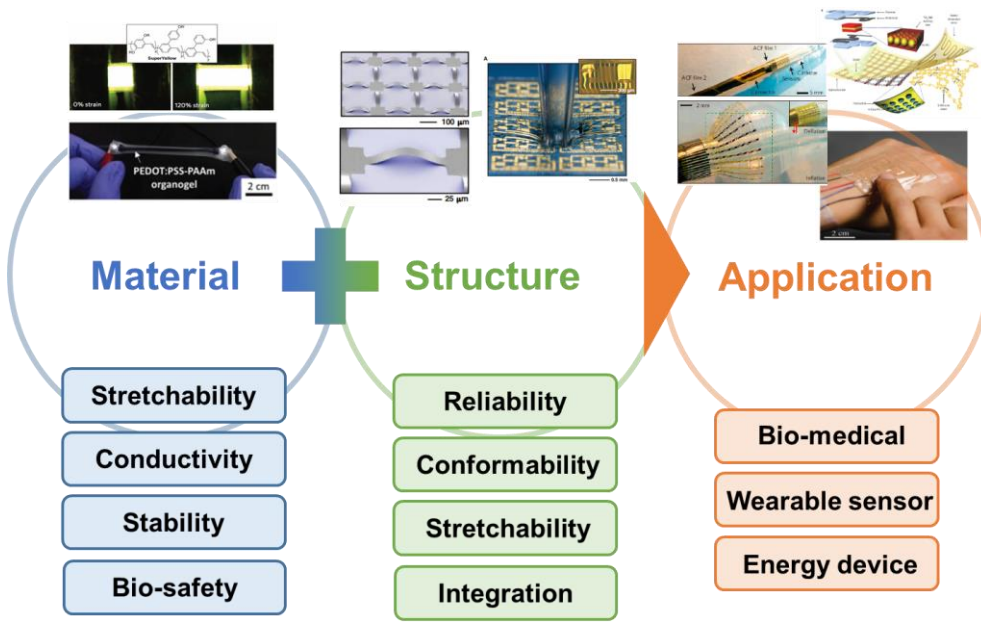

Figure 1.1 Strategies of manufacturing soft electronics: One for developing functional soft material, the other for developing the flexible design to relieve or avoid mechanical stress.

1.3 Auxetic: a new geometric concept for soft electronics

Metamaterials are generally referred to as 'meta-characteristics' because they could not be expressed by the theoretical common material behavior, including optical, mechanical, and thermal properties.[10-12] Meta-characteristics usually had a negative index, i.e. negative refractive index, negative compressibility. Actually, these unique material behaviors were characterized when they have a specific internal structure, rather than the material's own property.

A mechanical metamaterial was generally referred to as a material having negative mechanical parameters. In this thesis, we have investigated 'Auxetic', which could represent negative Poisson's ratio performance, as a new concept of structural material for flexible devices.[13] When a material was stretched in one direction, shrinkage occurred in a transverse direction to the stretching direction. Poisson's ratio of 3-dimensional isotropic materials can be defined as a negative ratio in the transverse strain to an axial strain,

$$\nu = -\frac{transverse\ strain}{axial\ strain} = -\frac{\varepsilon_y}{\varepsilon_x} = -\frac{\varepsilon_z}{\varepsilon_x} \qquad \text{(Eq. 1.1)}$$

where Poisson's ratio is an inherent mechanical characteristic of the material.

Therefore, a negative Poisson's ratio indicated that the material could expand together in a transverse direction when it was stretched in one axis. Conversely, contraction could occur in the transverse direction when the material contracts in the axial direction. The auxetic behavior came from the structural aspect, not the inherent mechanical properties

of the material. The tensile deformation morphologies of three-dimensional typical and auxetic materials were provided in **Figure 1.3**.

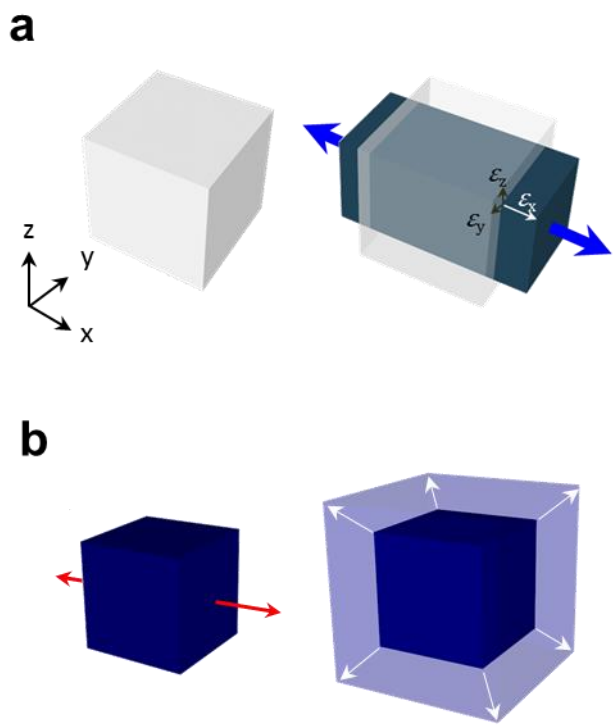

Figure 1.3 Tensile behavior of 3-dimensional (a) conventional materials (b) auxetic materials. When pulled, auxetic materials could also expand to transverse direction, thereby the volume of the auxetic could be increased.

Auxetics already have been widely used in various industries. Due to their biaxial expandability and compressibility, the auxetics could act as a filter. **Figure 1.4a** displayed an example of the application of an auxetic structure to architecture, in which the sunroof of the Al Bahar tower in Abu Dhabi, which was designed to control the magnitude of light incidence.

One more thing of the advantage of having a negative Poisson's ratio characteristic is that it could maintain a very good adhesive surface without buckling on a non-Gaussian plane. The Gaussian curvature could be calculated by the product of the two principal curvature, where for pristine positive Poisson's ratio materials showed saddle shape. For auxetics, they were easy to make synclastic surface when subject to a bending moment, because the outward plane could receive biaxial tension while the inward plane received biaxial compression. Based on this property, the auxetic structure could be also applied as a shape programmable material. The examples showing excellent conformal property of auxetic was represented in **Figure 1.4b** and **Figure 1.4c**.

Expandability and conformability aspects were an excellent fit for use as a platform for wearable, attachable devices. Based on these features, the auxetic structures were expected to be designed so that they could be deformed according to a user's desired direction.

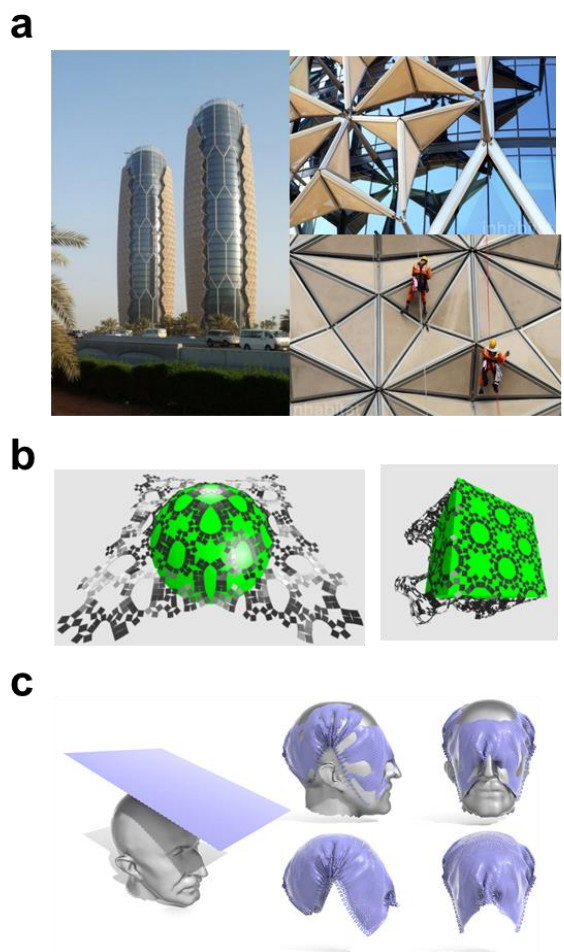

Figure 1.4 (a) Architecture application of auxetic structure as a sunroof in Al Bahar tower (b), (c) Examples showing excellent conformability of auxetic on rugged surface.[14, 15]

1.4 Objective of thesis

Studies on the auxetic had mainly been conducted on the mechanical properties, mainly reporting and analyzing the dependence of the auxetic behavior depending on the structural factors constituting the auxetics. Most of the researches related to auxetic engineering had been regarded as a study of architectural and mechanical behavior, and there were few reports on the application of such structure to electronic devices. In this thesis, we investigated the mechanical behavior of auxetics based on soft material and suggested a new paradigm as a structural material for flexible and stretching devices through simulation and experimental proof.

1.4 Organization of this thesis

This thesis consists of 5 chapters. In chapter 2, mechanical properties of materials were introduced to model the mechanical behavior of soft materials and auxetics. Chapter 3 described the strain-isolable characteristics of hierarchical rotating unit auxetic which could avoid mechanical stress during severe deformation. Based on the characteristics, extremely deformable batteries were developed as a proof of concept. In Chapter 4, full solid auxetic soft material was introduced through re-entrant auxetic composite. The elastic property including modulus and Poisson's ratio could be predictively controlled by the geometric design and material selection. The composite showed 2-dimensional semiauxetic property, therefore severe thickness shrinkage occurred during the stretch. This anisotropic deformation behavior improved the performance of capacitive type stretchable strain sensor where the sensing mechanism depended on the geometric change of dielectric. Chapter 5 summarizes the results of this thesis.

CHAPTER 2

Theoretical Background

2.1. Neo-Hookean solid

The relationship between stress and strain of soft elastomeric materials such as rubbers does not well following Hooke's law. A hyperelastic material is a type of ideally elastic material where the stress-strain relationship derived from a strain energy density function instead of Hooke's law. There are many kinds of models explaining hyperelastic, focusing on the microstructural perspective or continuum mechanics perspective.

A neo-Hookean solid is one of the hyperelastic models that can simply describe the soft material and is possible to predict the nonlinear stress-strain behavior of materials experiencing large deformations.[16] The initial stages of stress and strain shows a linear relationship and will plateau at a certain point. The neo-Hookean model is based on the statistical thermodynamics of cross-linked polymer chains and is usable for plastics and

rubber-like substances. Cross-linked polymers will act in a neo-Hookean manner because initially the polymer chains can move relative to each other when a stress is applied. However, at a certain point, the polymer chains will be stretched to the maximum point that the covalent cross links will allow, and this will cause a dramatic increase in the elastic modulus of the material. The neo-Hookean material model does not predict that increase in modulus at large strains and is typically accurate only for strains less than 100%.

The strain energy density function for neo-Hookean material in a three-dimensional description is

$$W = C_1(I_1 - 3) + D_1(J - 1)^2 \qquad \text{(Eq. 2.1a)}$$

Where C_1 is a material constant. If the material is incompressible, or $J = \lambda_1\lambda_2\lambda_3 = 1$, therefore the Eq. 2.1 can be expressed as

$$W = C_1(I_1 - 3) \qquad \text{(Eq. 2.1b)}$$

I_1 is a first invariant of the right Cauchy-Green deformation tensor, or

$$I_1 = \lambda_1^2 + \lambda_2^2 + \lambda_3^2 \qquad \text{(Eq. 2.2)}$$

Where λ_i is the principal stretches.

2.2. Theoretical limit in Poisson's ratio of isotropic material

Poisson's ratio of conventional 3-dimensional isotropic materials cannot exceed 0.5, which can be demonstrated by the volumetric calculation under pulling of a cubic body. Assuming that the initial volume of the cubic body is $V_0 = 1$, then the total volume after the pulling deformation will be expressed as:

$$V = (1+\varepsilon_x)(1+\varepsilon_y)(1+\varepsilon_z) \quad \text{(Eq. 2.3)}$$

If neglecting the multiplied strain component, the equation is approximated as:

$$V \approx 1+\varepsilon_x+\varepsilon_y+\varepsilon_z \quad \text{(Eq. 2.4)}$$

The volume can not be exceed the initial value, in other words, $V \leq V_0$. For istropic material, $\varepsilon_y = \varepsilon_z$. Therefore,

$$\varepsilon_x + 2\varepsilon_y \leq 0 \quad or \quad v = -\frac{\varepsilon_y}{\varepsilon_x} \leq 0.5 \quad \text{(Eq. 2.5)}$$

Therefore, the closer the materials are to incompressibility, the less the volume changes during deformation. From this relationship, an upper limit of Poisson's ratio can be obtained.

When an external force is applied, a general elastomer easily deforms instead of being compressed, and try to maintain a constant volume at the time of deformation, so that it

has a Poisson's ratio of 0.5. (0.3~0.4 for metal)

The relationship between shear moduli and Young's moduli is followed by:

$$G = \frac{E}{2(1+v)} \qquad \text{(Eq. 2.6)}$$

$$v = \frac{E}{2G} - 1 \qquad \text{(Eq. 2.7)}$$

Since $E, G > 0$, $v > -1$

Therefore, the theoretical limitation of *Poisson*'s ratio of 3-dimensional isotropic materials are $-1 < v \leq 0.5$.

2.3. Auxetic

2.3.1. Classification of auxetic

There are several types of structures which could lead to auxetic behavior, regardless of dimensions. In this thesis, only 2-dimensional auxetic structure will be referred. The conventional 2-dimensional auxetic structure can be divided into three groups based on their hinging mechanism: re-entrant, rotating unit, and chiral. Each structure has a different auxetic mechanism and areal densities, therefore the equivalent modulus and Poisson's ratio is different. Schematic illustrations of three representative auxetic structure are given in **Figure 2.1**.

Figure 2.2 showed equivalent Young's modulus and Poisson's ratio of several auxetic structures, which was analyzed by computer modeling by Elipe et al., Besides the different hinging mechanism, the elastic properties of auxetic structure could be changed even within the same group.[17] The dependence of geometric factor on the *Poisson*'s ratio of re-entrant auxetic would be discussed in chapter 2.3.3 in more detail.

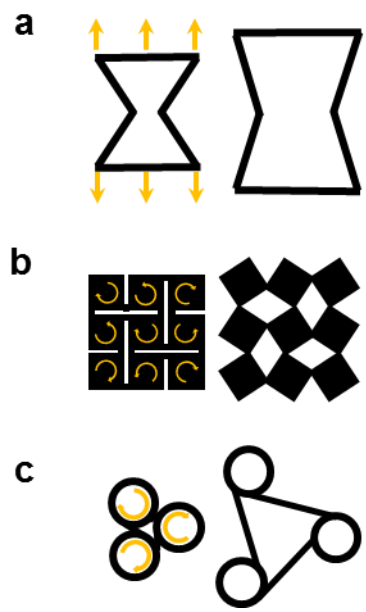

Figure 2.1 Representative structures of 2-dimensional auxetic. There were many ways to realize auxetic property as illustrated in Figure. (a) Re-entrant auxetic (b) Rotating unit auxetic (c) Chiral auxetic. When stretched, the hinges in the auxetic rotated and finally could be expanded in transverse direction.

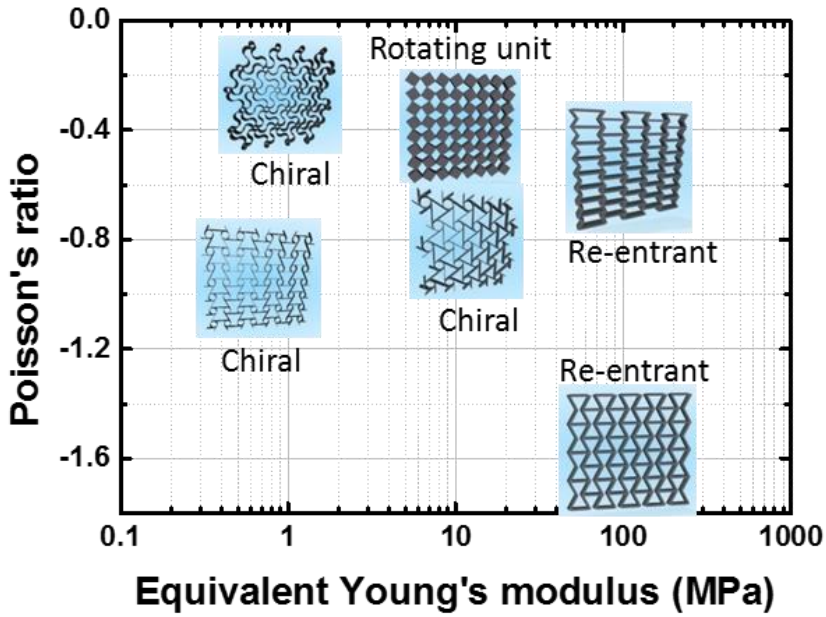

Figure 2.2 Equivalent Young's modulus and Possion's ratio of vairous kinds of auxetic structure. Even though the mechanism of auxetic behavior was similar, the mechanical property could be greatly changed by geometry.[17]

2.3.2. Mechanical models for re-entrant auxetic structure

Figure 2.3 is a symmetric unit of re-entrant auxetic structure. The mechanical property of auxetic structure can be determined by their geometric factors. In this case, the unit width *w*, diagonal length *h*, and the rib thickness *t*, and re-entrant angle θ.

If the auxetic behavior of re-entrant structure is able to be achieved by the hinging motion only, the Poisson's ratio can be expressed as,[18]

$$v_{yx} = \frac{\sin\theta(0.5w/h + \sin\theta)}{\cos^2\theta} \qquad \text{(Eq. 2.8)}$$

If the re-entrant auxetic will be consist of flexural elements, then additional motions including hinging behavior occur at the re-entrant auxetics. The three kinds of deformation model in re-entrant auxetics are illustrated in **Figure 2.4**.

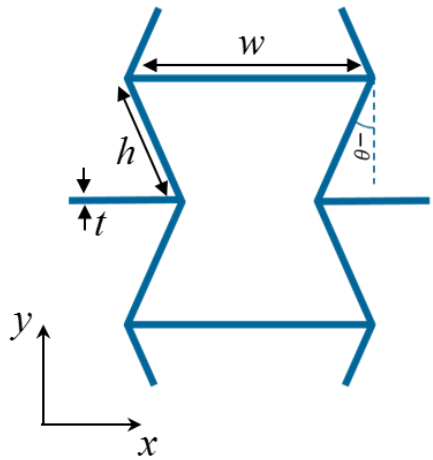

Figure 2.3 Geometric variables determining the mechanical property of re-entrant auxetic structure.

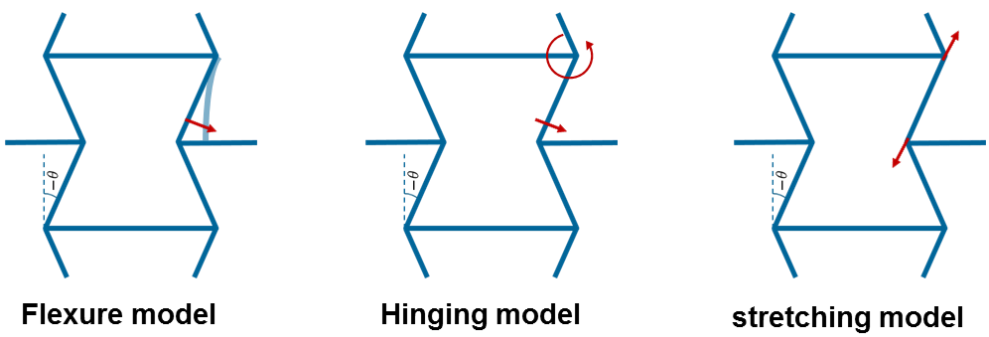

Figure 2.4 Three kinds of motions driving auxetic behavior in re-entrant structure. In this case, the Flexure model and hinging model can induce the auxetic property of re-entrant structure.

2.4. Mechanism of capacitive type strain sensor

A strain sensor is a device which can measure the amount of strain quantitatively when mechanical deformation occurs. Strain sensor could be divided into two vary on their measurement type: one is a capacitive type and the other is a resistive type. For capacitive type strain sensors, the change of capacitance was measured during the deformation. When external force applies to the capacitive type sensor, the geometry of the flexible dielectric can be deformed and results in the capacitance change. Resistance is measured during deformation instead of capacitance for resistive type sensor. Gauge factor, which is the ratio of capacitance change ratio to strain, is a performance criterion of strain sensor.

The capacitance of initial 3-dimensional isotropic dielectric can be calculated as:

$$C_0 = \varepsilon_0 \varepsilon_r \frac{A_0}{d_0} = \varepsilon_0 \varepsilon_r \frac{x_0 y_0}{z_0} \qquad \text{(Eq. 2.9)}$$

The capacitance change of 3-dimensional isotropic dielectric under stretching deformation can be derived by:

$$C = \varepsilon_0 \varepsilon_r \frac{x_1 y_1}{z_1} = \varepsilon_0 \varepsilon_r \frac{x_0(1+\varepsilon_x) y_0 (1+\varepsilon_y)}{z_0(1+\varepsilon_z)} = C_0 \frac{(1+\varepsilon_x)(1+\varepsilon_y)}{(1+\varepsilon_z)} \qquad \text{(Eq. 2.10)}$$

Because the dielectric is isotropic, $\varepsilon_x = \varepsilon_z$. Therefore,

$$C = C_0(1+\varepsilon_y) \quad or \quad \Delta C / C_0 = \varepsilon_y \qquad \text{(Eq. 2.11)}$$

From Eq. 2.11, the gauge factor of 3-dimensional isotropic dielectrics can show 1, regardless of the material type. For conventional capacitive type sensors, the linear relationship between capacitance change and strain is a great advantage in addition to the fast response, however, fixed the value of gauge factor is a fundamental limitation compared to the resistive type which could be controlled even more than 10^2.

CHAPTER 3

Hierarchical Auxetics for Extremely Deformable Device Platforms

3.1. Introduction

Rotating unit based self-similar hierarchy had been recently intensively investigated as a mechanically reconfigurable metamaterials.[15, 19-22] As the auxetic had a self-similar hierarchy, the expandability of whole structure could increase more as the level of hierarchy increased, as noticed in **Figure 3.1**.[15] Previous literature reported that the stiffness and *Poisson*'s ratio of hierarchical auxetic could be engineered by appropriately arranging the hierarchical design and also could be used as shape programmable material because the degree of freedom of final shape determination exponentially increased.

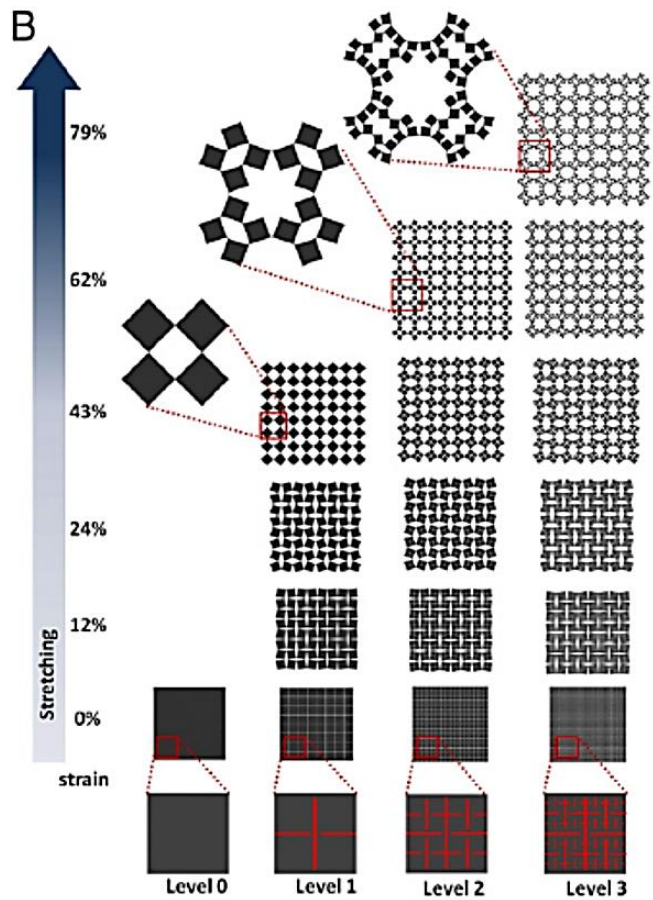

Figure 3.1 Schematic illustration of hierarchical rotating unit auxetic and their stretchability depending on the hierarchy level.[15]

Because the hinges connecting the rotating unit behaves rotating motions in conventional rotating unit auxetic, two-dimensional expansion could be achieved even though the units consisted of rigid material. When a rotating unit auxetic is fabricated by soft material, the hinge has a finite dimension as shown in **Figure 3.2**. Interesting thing is that when the rotating auxetic expanded, the strain could only be isolated in the hinges rather than unit, which was already reported by Tang et al.[19] The ability to intentionally design the point where the deformation occurs and the area that does not occur with such a wide expansion rate shows the possibility that it can be used as a platform for a flexible device.

However, the deformation behavior of the existing hierarchical auxetic has been studied only for the two-dimensional expansion. When fabricating it through a soft material, the hierarchical auxetic may also involve three-dimensional deformation. That is, if the strain isolation effect can be induced in three dimensions in a similar manner to that in the two dimensions, the hierarchical auxetic was expected to operate as a freely deformable flexible device platform in all directions.

In this study, it was firstly investigated that whether the strain could be selectively isolated only in the hinge region even if the soft material based hierarchical auxetic manufactured was subjected to complicated deformation. In addition to verifying the reliability of the material, we propose a new paradigm for flexible device platforms.

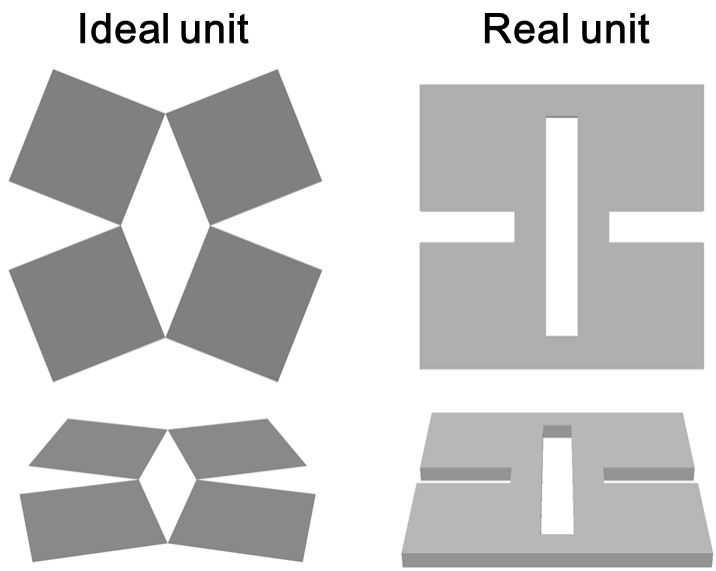

Figure 3.2 Rotating unit auxetic having ideal hinge (width=0) and the real hinge. Mechanical stress can be generated in real hinge when the auxetic expand.

3.2. 3-dimensional deformation of soft hierarhchical auxetic

Deformation concept of our motif cut fabricated by soft materials was presented in **Figure 3.3**. **Figure 3.3a** showed a typical expanding motion of level-1 hierarchical auxetic structure, which was made of rigid stainless steel. The individual rigid square unit could be rotated by 45 degrees around rotational hinges and consequently created the expanding motion. In this case, the inherent elasticity of the unit material is regardless. Interestingly, the ability of deformation of hierarchical auxetic structure could become more diverse if manufactured in soft material. **Figure 3.3b** represented the deformation concept of motif cut fabricated by conventional rubber. When the hinges became flexible, the auxetic could possess additional freedom in 3-dimensional deformation such as bending and twisting as presented in Figure 3.3b in addition to stretching behavior. In this case, the soft hinges played an angular joint role to let the square unit cells move in a various direction. Owing to these newly created deformation abilities, our hierarchical auxetic is expected to switch its shape in response to external compressive stress and furthermore, it could even be crumpled which is considered as an extremely deformed state.

Before analyzing the deformation behavior of hierarchical auxetic structure, the validity of the auxetic motif was performed. **Figure 3.4a** showed the three comparable models; one is a pristine sheet, another is auxetic cut motif, the other is the cross cut pattern having same cut density with auxetic cut motif. The three models underwent bending and twisting to see the strain isolation effect and to judge the ease of deformation. **Figure 3.4b and 3.4c** represented the maximum principle strain contour of three models after the same magnitude of bending and twisting. Among three models,

only the auxtic cut model can effectively isolate the strain during the deformation, while others experienced distortion of entire structure especially in twisting behavior. To achieve the same degree of deformation, auxetic cut model required the lowest force or moment to be bent or twisted as illustrated in **Figure 3.4d**, which indicated that they were the most deformable with little force. Therefore, the hierarchical auxetic motif might be excellent and optimized design for the deformable platform.

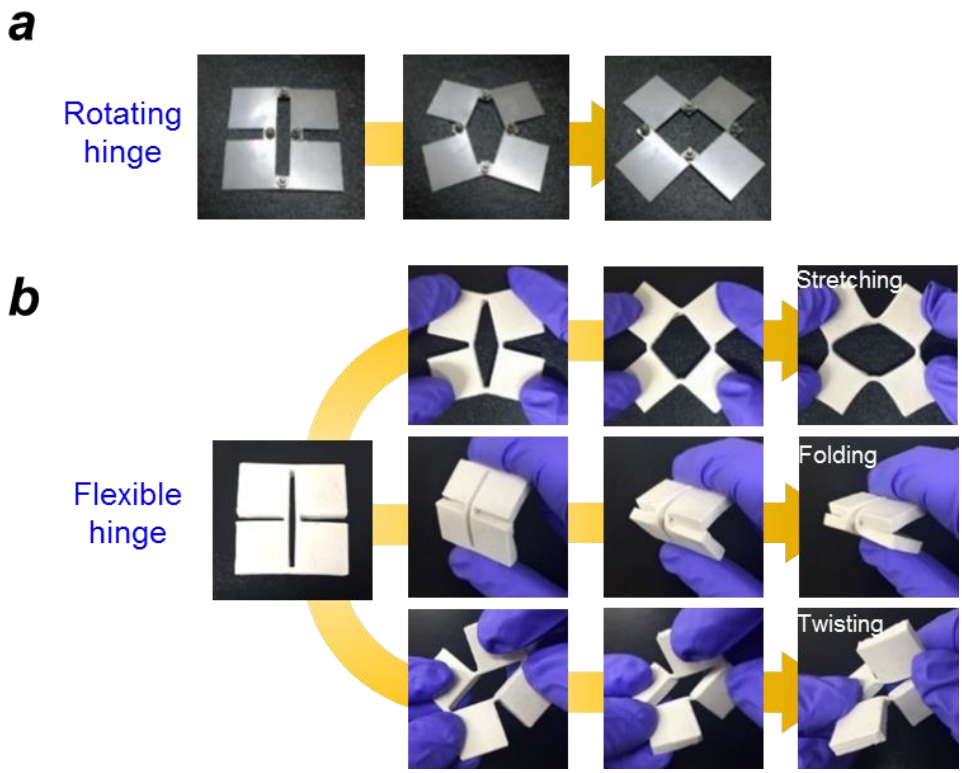

Figure 3.3 (a) Expansion behavior of level-1 hierarchy auxetic by the motion of conventional rotating hinge. (b) Advanced deformability of level-1 hierarchy auxetic using flexible hinge. By adopting flexible hinge concept, the fractal cut could show 3-dimensional deformation such as folding, and twisting, which indicate that the hinges could have infinite degree of freedom in deformation.

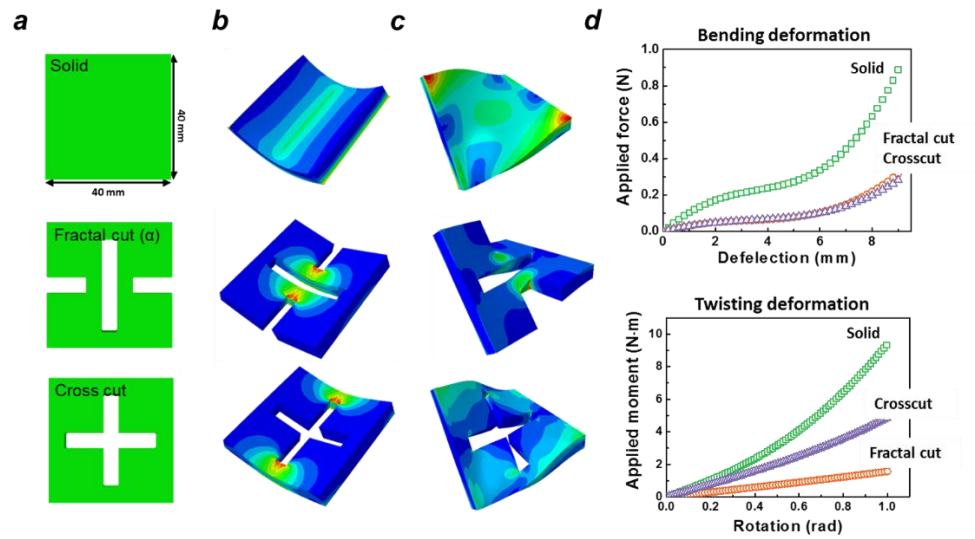

Figure 3.4 Bending and twisting of three models for validity of fractal cut motif. (a) Candidate models including no cut, fractal cut, and cross cut. (b), (c) Maximum principle strain contour of three models under bending and twisting. (d) Force and moment v.s. deflection and rotation curve.

The design of auxetic cut motif is becoming more variable when providing hierarchy concept. **Figure 3.5** is the structural map of hierarchical rotating unit auxetic. Their shape could be determined by the size of the unit and hierarchy level.[15] The scale of the deformable hinges in each model is all same, regardless of hierarchy level of the position. Even though the hierarchy level of the whole model is same, the number of hinges could differ: The number could increase when the size of the rotating unit decreased. Strain distribution property of hierarchy auxetics could be vary depending on unit size and hierarchy level.

Figure 3.6 showed the deformation characteristics of soft material based fractal cut varying on the hierarchy level. The higher amount of expansion and volumetric contraction could be achieved as the level of the hierarchy of auxetic increased. When crumpled, the pristine sheet had large recovery force to be flatten compared to the hierarchy auxetic structure, which indicated that the required force to deform was more difficult. More interesting characteristics of hierarchy auxetic were the excellent conformability on a non-zero Gaussian surface. It was difficult for a pristine sheet to cover the curved surface without delamination while the fractal cut material could show perfect adherence because the pristine sheet could remain stable when the Gaussian curvature is 0 as aforementioned in background theory at chapter 1. Therefore, hierarchy auxetics fabricated by rubbers seemed to be worth for making omnidirectionally flexible structures, considering the advanced deformability possible to accommodate external compressive stresses as well as tensile stress.

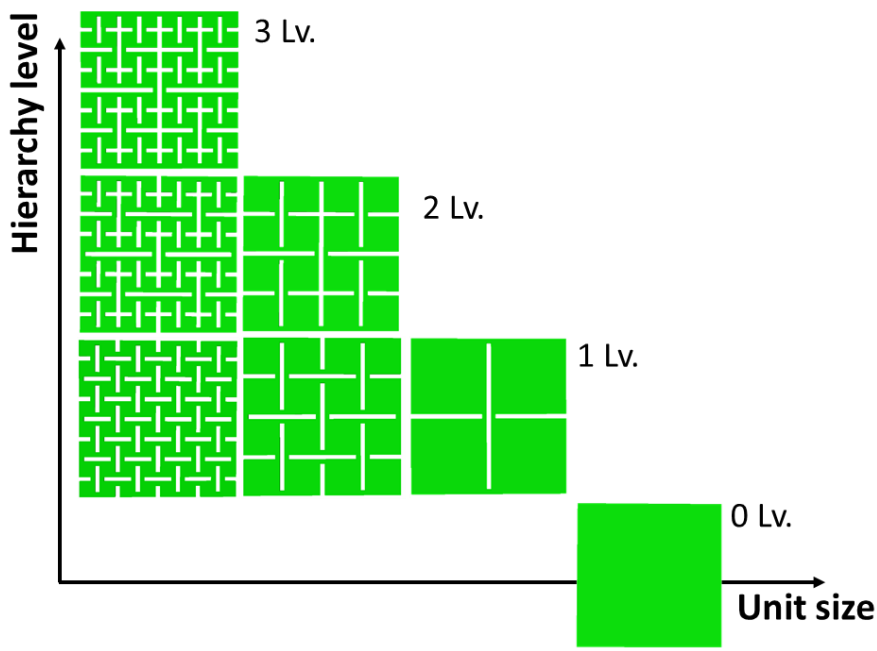

Figure 3.5 Structural map of hierarchy auxetic depending on the unit size and hierarchy level. Hierarchy auxetic which includes small unit is a multi-lattice structure of unit motif.

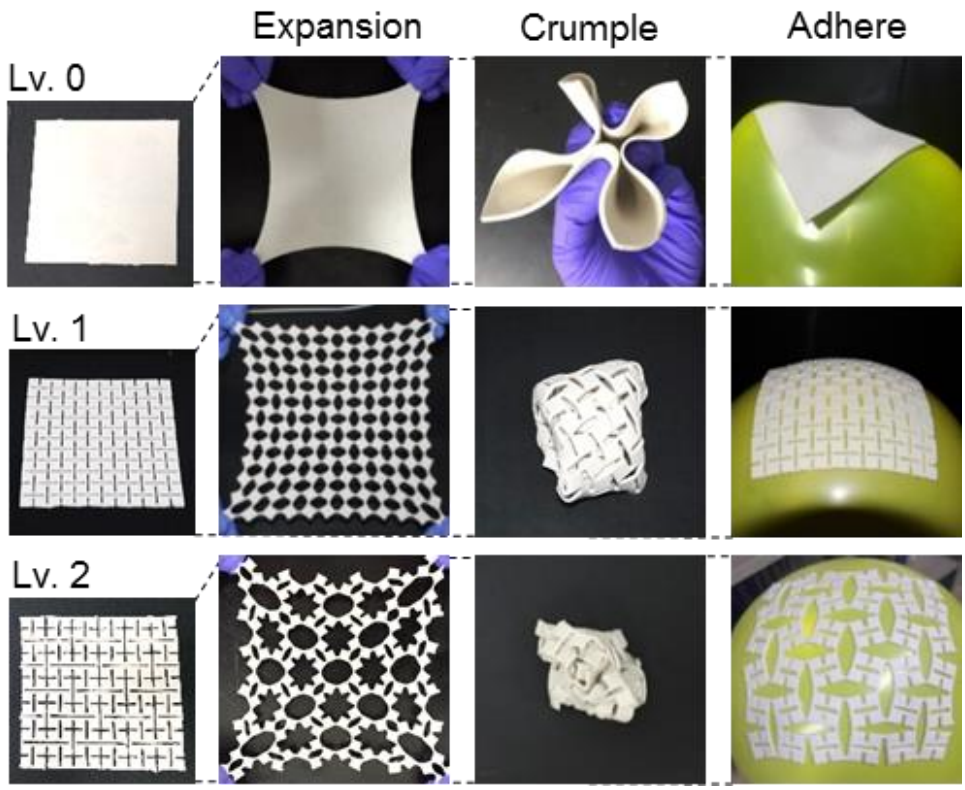

Figure 3.6 Deformability of fractal cut lattice depending on hierarchy level. As the hierarchy level increased, fractal cut could possess enhanced stretchability, contractability, and excellent conformability.

In this work, we developed omnidirectionally and extremely deformable structural materials focusing on the strain isolation, inspired by hierarchical auxetic structure. In order to apply the hierarchical auxetic to a platform for a flexible device, it is necessary to verify that the device can avoid mechanical failure when an external force is applied. We demonstrated for the first time that soft-material-based hierarchical auxetic structures could maintain effective strain isolation property even under complex deformation in three dimensions, and then could be used as an extremely deformable device platform. In this case, the soft hinges consisting the hierarchical auxetic design acted as an unstable singular point in deformation perspective, and contributed to the effective strain-isolation behavior and enhancing the deformability. Based on the deformation characteristics, we applied a hierarchical auxetic structure to produce a battery that can operate stably even under complex and large deformations such as tension and crumpling.

3.3. Experimental procedure

Experiments were divided into three parts; first, the mechanical reliability confirmation of single hinge was performed. Secondly, deformable batteries were fabricated based on the silicon rubber based level-3 hierarchical auxetic structure, to verify the potential ability of extremely deformable device platform. Hierarchical shape cast was fabricated through 3-dimensional printing, and then as-prepared pouch cells were properly aligned on the printed mold with series and parallel electrical connection. After that, silicon rubber resin was molded in the cast with covering the aligned pouch cells, and finally fabricated level-3 hierarchical auxetic battery after solidification. The process step of battery fabrication was illustrated in **Figure 3.7a**.

In particular, it was important to align the cell in the unit region to avoid distortion. **Figure 3.7b** showed the schematic illustration of an internal structure of battery in more detail. The simplified model is composed of one joint hinge and a pair of lithium ion cells, and the cells were connected with each other in a parallel connection using PVC wrapped Cu wires. The cells should be placed far away from hinge where strain generated. At this time, we positioned the junction between Cu wire and cell (+), (-) terminals of cells apart from the hinges as possible. Li-ion battery consisted of $LiNi_{0.8}Co_{0.15}Al_{0.05}O_2$ (NCA) - artificial graphite full cells were used.

Beyond the elastomeric packaging material, we applied the hierarchical auxetic design to plastic thin film devices. The hierarchical auxetic structure was patterned in polyethylene Terephthalate (PET) substrate, which is conventionally used material in the bendable device. In the present research, we tried to fabricate screen printed battery on PET substrate. Battery elements such as carbon current collector, anode and cathodes,

electrolyte slurries were prepared and printed on PET substrates in series. The schematic of level-1 hierarchical auxetic printing battery was provided in **Figure 3.8**.

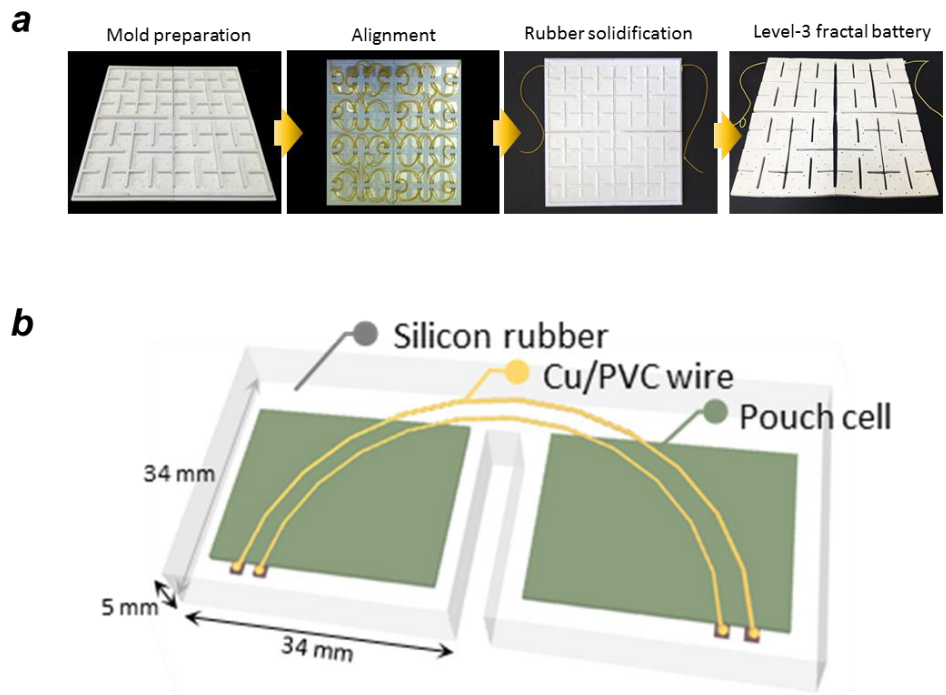

Figure 3.7 (a) Manufacturing process of Level-3 hierarchical auxetic battery. (b) Schematic illustration of the internal array of auxetic battery. Pouch cells were placed in the unit region to avoid mechanical deformation.

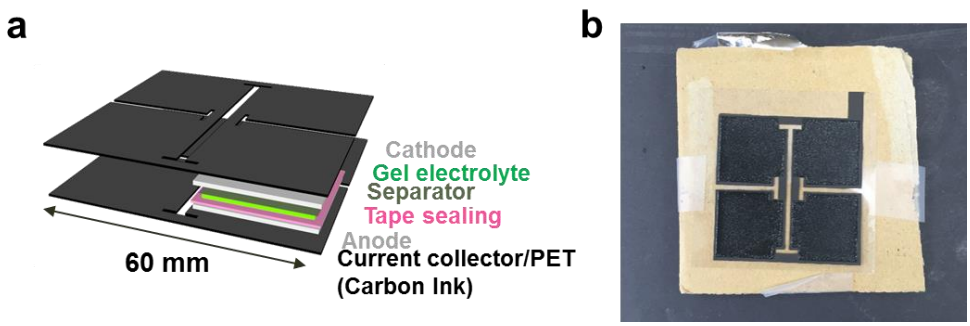

Figure 3.8 (a) Schematic illustration of screen printing battery with level-1 hierarchy structure. (b) Current collector/anode printed on patterned PET substrate.

3.4. FEM for 3-D deformation of hierarchical auxetic

It is necessary to check whether a strain-isolation occurs in a hinge during complex deformation in order for a soft material based hierarchical auxetic to be used as an extremely deformable device platform. To verify the strain-isolation effect, we first observed the strain distribution of hierarchical auxetic which underwent complicated deformation through finite element analysis. To find out the optimum structural design for effective strain-isolation, we examined the deformation behavior of hierarchical auxetic depending on the hierarchical level. For numerical analysis, mechanical properties of conventional rubber were applied as a Neo-Hookean model for a hyperelastic property (The C10 and D1 coefficients of Neo-Hookean model were 0.068 and 0.007). Applied mesh elements were C3D8 for a hinge, and C3D4 for a unit. Uniaxial tensile deformation and crumpling deformation were performed through static and explicit analysis. The applied deformation direction was illustrated in **Figure 3.9**.

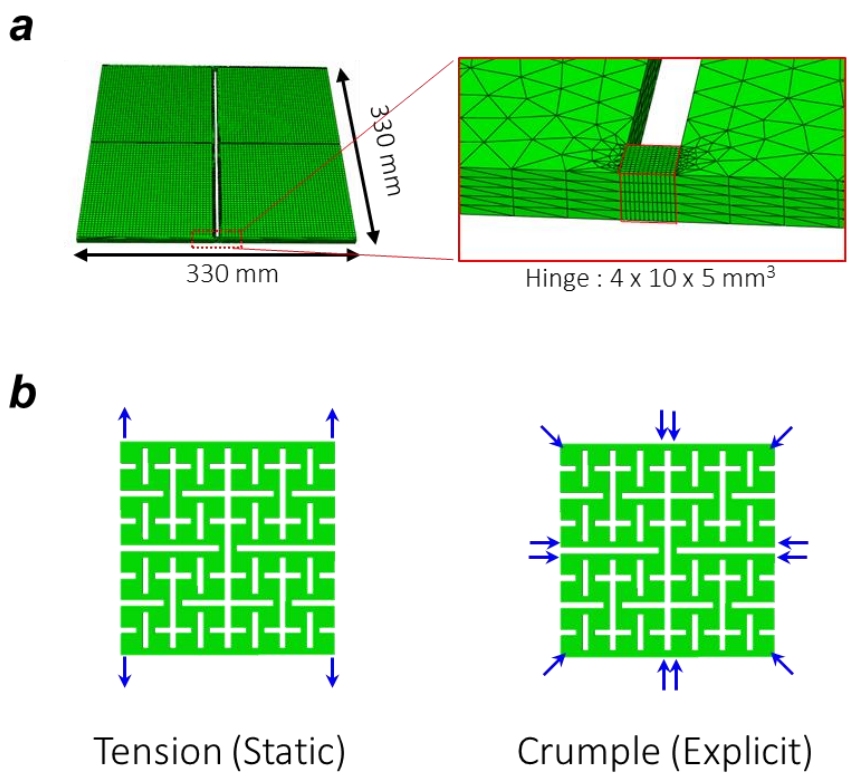

Figure 3.9 (a) Scale and mesh information of hierarchical auxetic. (b) Applied load condition to the tensile and crumple model.

3.4.1 Tensile deformation model

Figure 3.10 was the FEM simulation results of mechanical behavior of hierarchical auxetics. In the case of tensile deformation, a static analysis was performed by applying an equal force in the uniaxial direction to both ends of auxetic. To compare the hierarchy level dependence accurately, the size of sub-unit was fixed to be similar. We compared the strain energy density of individual fractal cut model to figure out the dependence of hierarchy level on deformability. **Figure 3.11** denoted that the increasing level of hierarchy improved the stretchability. At the same degree of elongation, the strain energy density was measured to be decreased as the level of hierarchy increased or in other words, the stiffness of hierarchy auxetic decreased. The strain contour represented that hinges in hierarchical auxetic mainly trapped the generated strain regardless of the hierarchy level. Of a number of hinges, the maximum strain occurred in the hinge of the motif corresponding to the level-1, denoted by the red arrow. The maximum strain of the auxetic with different hierarchy level was compared in **Figure 3.12** when equally tensioned to 25 %. The magnitude of strain in the motif corresponding to the level-1 hinges decreased gradually when the hierarchical level increased. A motif of a higher hierarchical level was opened during the stretch, so that the concentrated stress at the level 1 hinge could effectively be dispersed. Therefore, higher hierarchy level would be the more favorable platform for tensile deformation perspective.

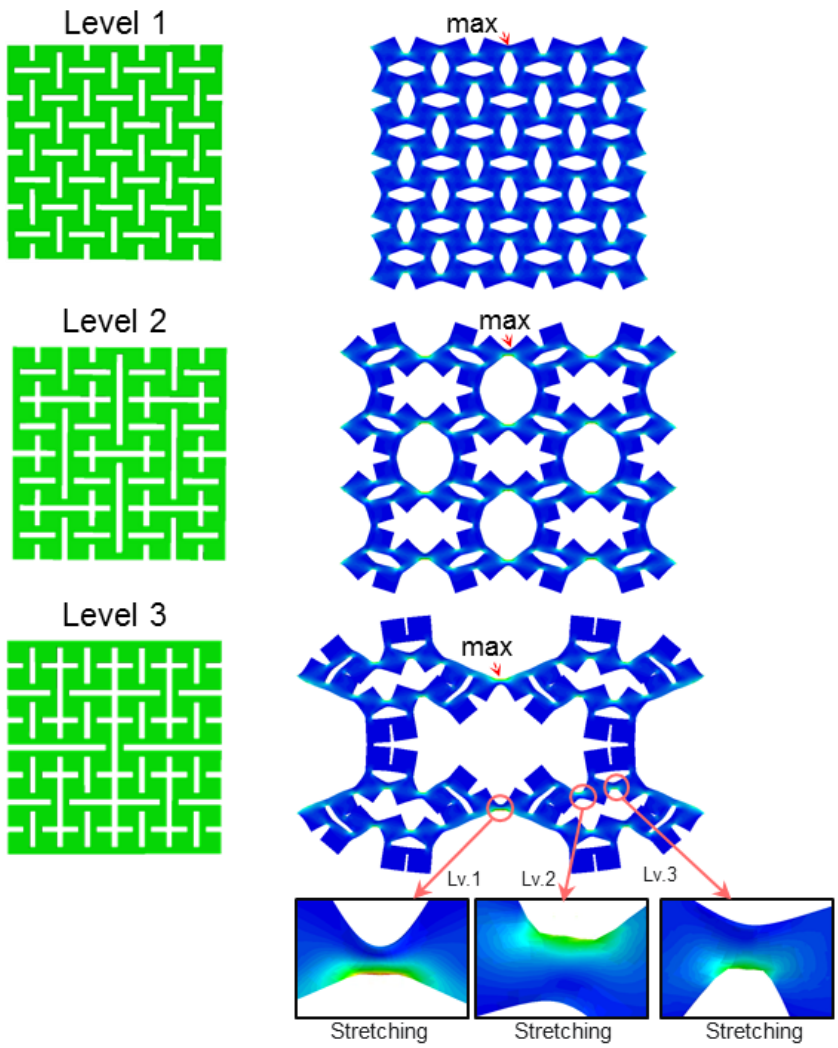

Figure 3.10 Maximum principle strain contour of level 1 to 3 of hierarchical auxetic. Strain-isolation effectively occurred at the hinge. The sites where the maximum strain occurred were the lowest level of hinge.

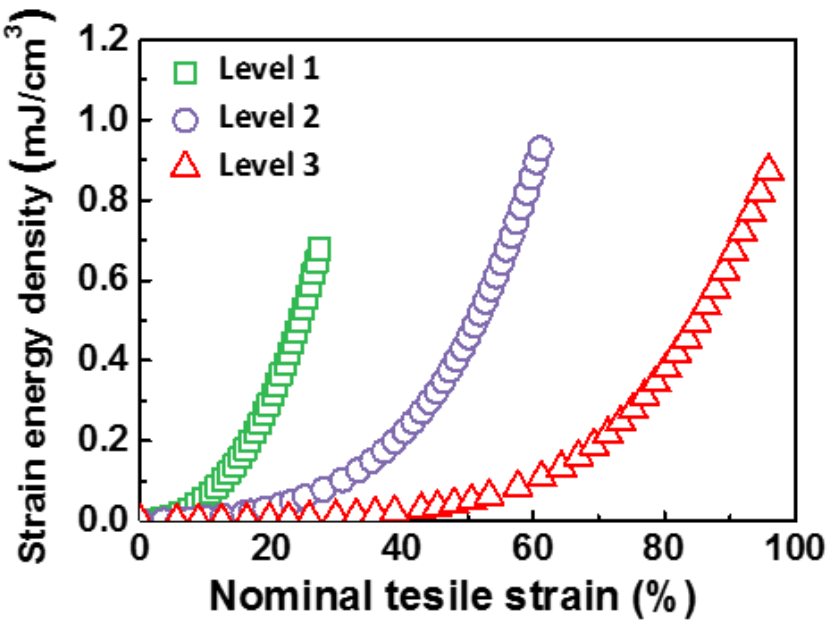

Figure 3.11 Strain energy density and deformation morphology of hierarchy auxetic elastomer during stretching. When same magnitude of force was applied, degree of elongation increased as hierarchical level increased.

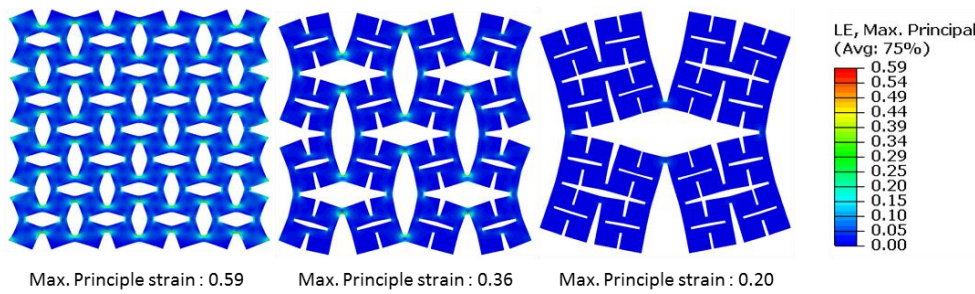

Figure 3.12 Maximum principle strain contour of individual hierarchical auxetic at the lowest level of hinge at 25 % stretching. Magnitude of maximum strain decreased as hierarchy level increased, due to the stress distribution of hinges positioned at the higher level.

3.4.2 Crumple deformation model

We observed that hierarchical auxetic was more easily crumpled as the hierarchy level increased, which was similar results in stretching model. Little distortion was observed in the rotating unit during crumpling, and the deformation was mostly concentrated at the hinges as displayed in the strain contour in **Figure 3.13**. Stretching, bending, and twisting occurred at the hinges, where the deformation modes were already predicted in Figure 3.3. From **Figure 3.14**, the strain energy density of hierarchical auxetic decreased as hierarchy level increased at the same magnitude of the crumpled state. This results indicated that the hierarchical auxetics required less force to be deformed.

When the hierarchical auxetic crumpled, the hinge served as a singularity point where distortion easily occurred. In this case, the hinges considered being similar to the role of apex in determining the shape of a crumpled paper.[23] The crumpling step of paper is similar to hierarchical auxetic; the paper was firstly wrinkled and formed several creases. When the deformation progressed, the formation of creased pattern intersected each other and vertexes were generated. These vertexes acted as singularity sites of deformation in paper crumpling. The only difference of the paper crumpling and hierarchical auxetic crumpling is that the hinges are intentionally designed sites while the vertexes were inevitably created sites.

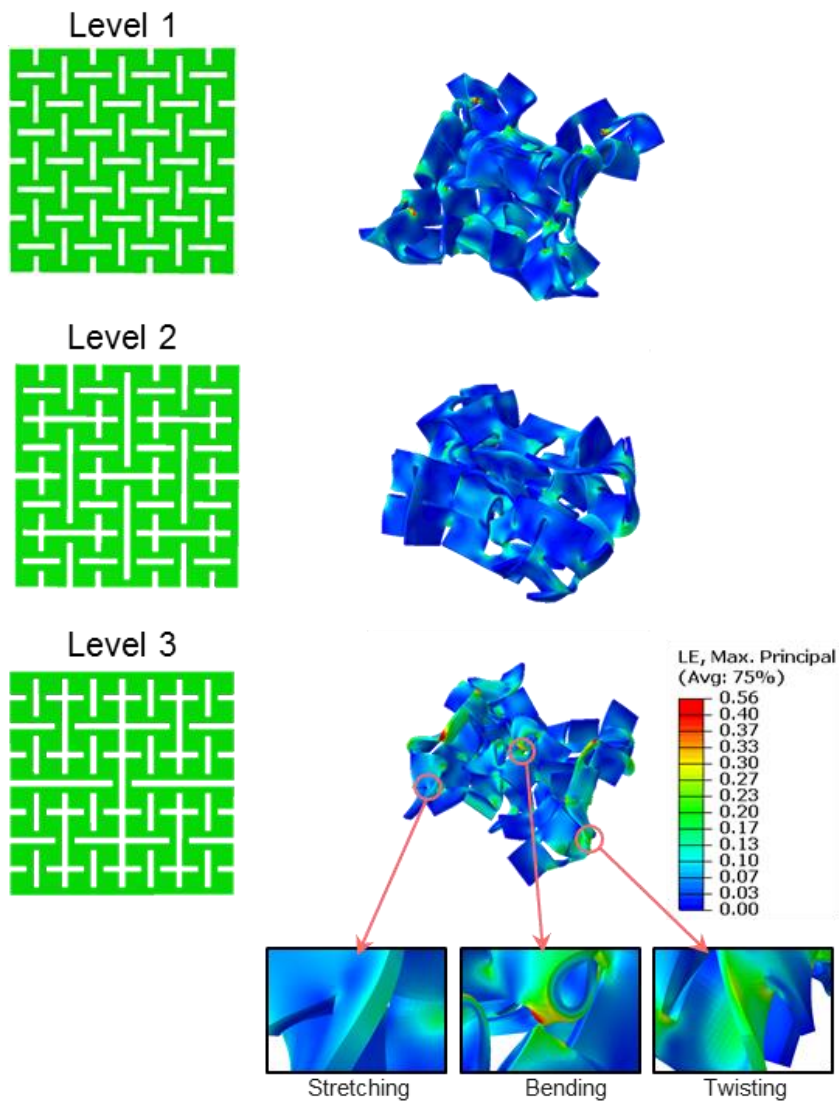

Figure 3.13 Maximum principle strain contour of level-3 fractal under crumpling. Hinges acted as an instable singular point during deformation, Individual hinge could undergo bending, twisting, and stretching.

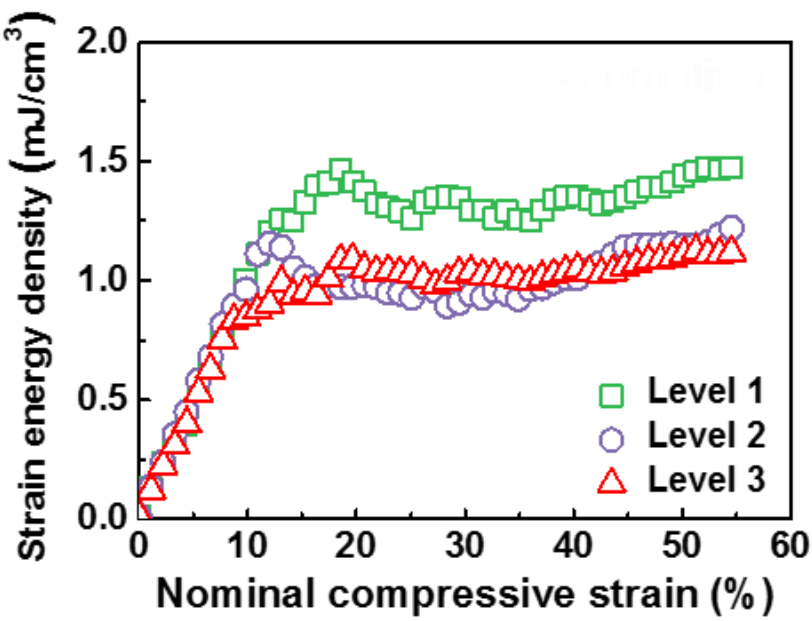

Figure 3.14 Strain energy density and deformation morphology of hierarchical auxetic elastomer under crumpling. Strain energy density decreased as the hierarchy level increased, indicating that they could be distorted more in ease.

A large compressive stress was first generated in the hinge corresponding to the level-1 motif which is considered to be a relatively narrow cross-sectional area, and the entire hierarchical auxetic could be crumpled by bending and twisting of hinges. The deformation step of hierarchical auxetic under crumpling.

The crumpling deformations of the hierarchical auxetic can be divided in step by step. **Figure 3.15a** shows the structure of auxetic having a level-3 hierarchy. When compressing the auxetic, the largest compressive stress is applied to the level-1 motif. In particular, the cut density is largest at the red dash line depicted in Figure 5.15a, therefore it is expected to be easily bent along this line. It is found from Figure 5.15b that it really folds at first a red dash line on under 10% nominal compressive strain condition. As the crumpling became severe, the hinges corresponding to the second level motif are also subjected to stress, which gradually deforms as additional buckling occurred. In this case, the strain was still concentrated on the hinge, while there was almost no distortion in the unit.

Square units can undergo distortion if their scales are too large, as presented in **Figure 3.16**. The two models had a same level-1 hierarchy but different square unit scale. Therefore, it is also important to consider the proper scale of the units in addition to hierarchical design.

Therefore, increasing the number of hinges according to the increase of hierarchy level led to lowering strain energy density of hierarchical auxetics, which indicated that the structure is easier to deform. In conclusion, it is desirable for hierarchical auxetic to have a higher hierarchical level in order to make easier to deform and preventing excessive stress concentration in the hinges.

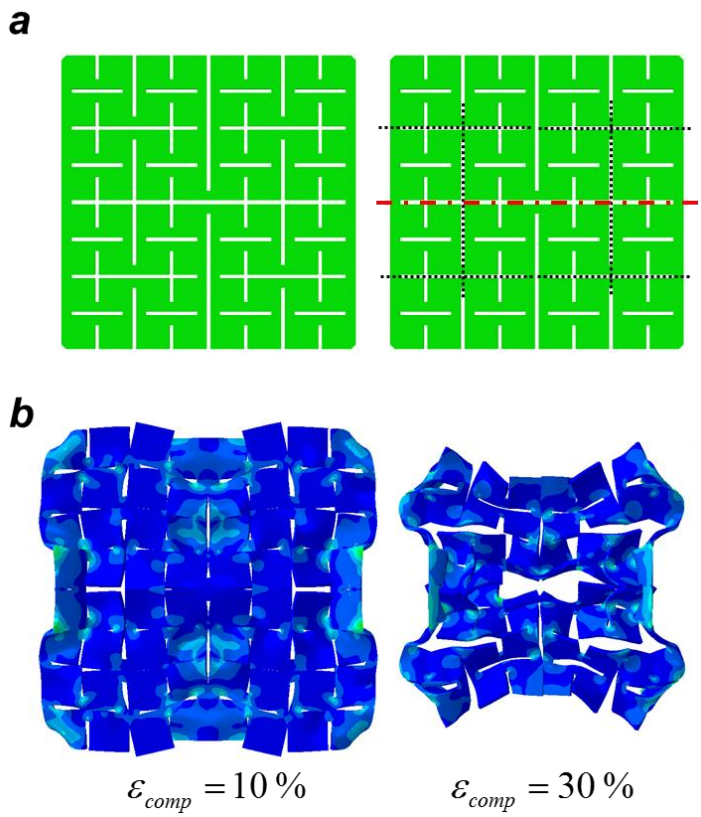

Figure 3.15 (a) Predicted crease sites when hierarchical auxetic crumpled as noted in red dashline and black dashline. (b) Crumpled state of level-3 hierarchical auxetic under compression.

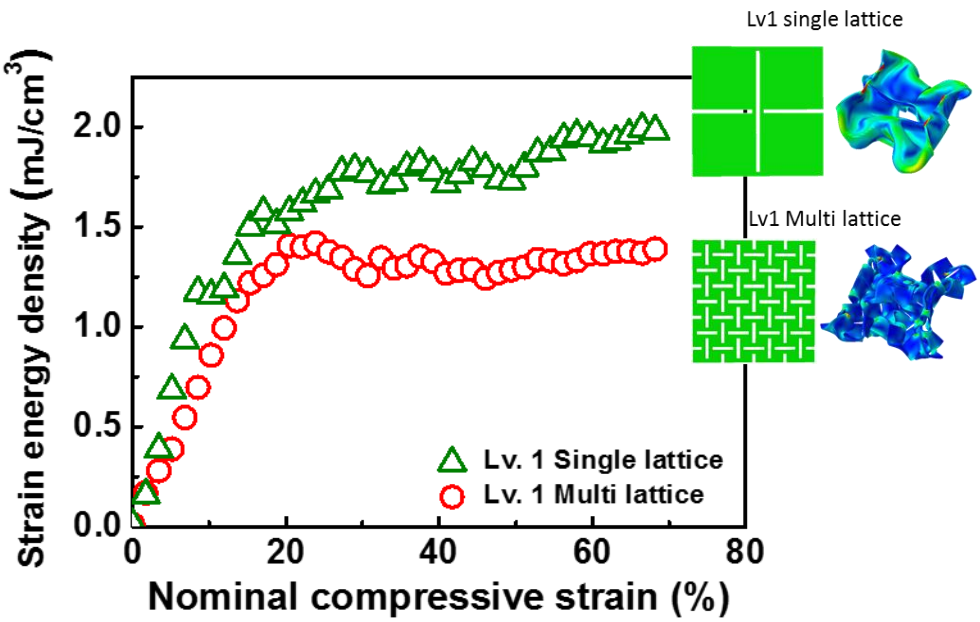

Figure 3.16 Strain energy density of crumpling depending on the geometric design of hierarchical auxetic model. Design containing high level hierarchy could be less stressed when distorted, even having similar subunit size. Though the same hierarchy level, the level 1 lattice structure had high cut density than level 1 single unit structure. Therefore, it is desired to have high hierarchy level with small subunit size for deformation perspective.

3.4.3 Motif array dependence

The lower level motif of hierarchical auxetic can have different array when the basic motif rotates in 90 degrees. **Figure 3.17** showed the schematic illustrations of level-2 hierarchical auxetic having different motif array and their strain energy curve during stretching. The α-β array model represented less strain energy compared to the α-α array, or in other words, the α-β array had smaller stiffness than the α-α array. The difference in stiffness indicated that the maximum expandability of hierarchical auxetic would be enhanced more when proper motif array is designed.

Motif array can also affect the mechanical stress state of a hinge. To see the magnitude of the stress of the individual hinge, volume averaged stress was calculated from numerical results, as illustrated in **Figure 3.18**. The green number noted the index of hinges corresponding to the level-1 motif, and the orange number noted the index of hinges corresponding to the level-2 motif. From the results, most of the stress concentrated on the hinges in the central position in α-α array case, where the hinge experienced bending and stretching. On the other hand, the hinges of α-β array effectively distributed the concentrated stress properly. The results indicated that hinges are possible to endure the generated stress under the same magnitude of the stretch. Therefore, it would be desirable to consider the array of motif for hierarchical auxetic in mechanical reliability perspective.

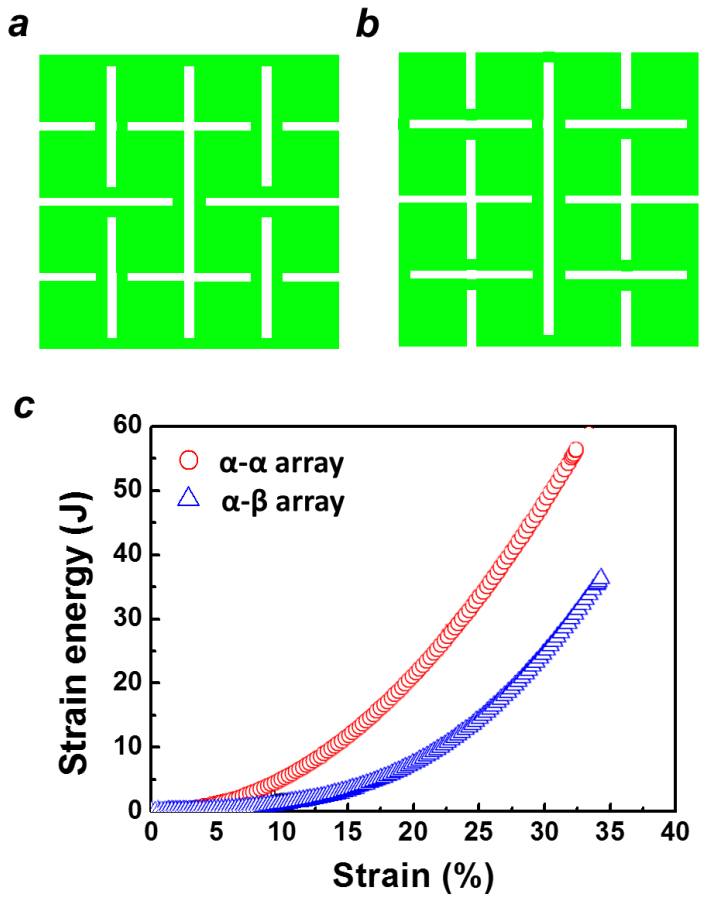

Figure 3.17 Level-2 hierarchical auxetic structure of (a) *α-α* array and (b) *α-β* array. Both model have same magnitude of volume (or cut density). (c) Strain energy curve during the stretch of *α-α* and *α-β* model. The results indicated that the *α-β* model had greater expandability than *α-α* model.

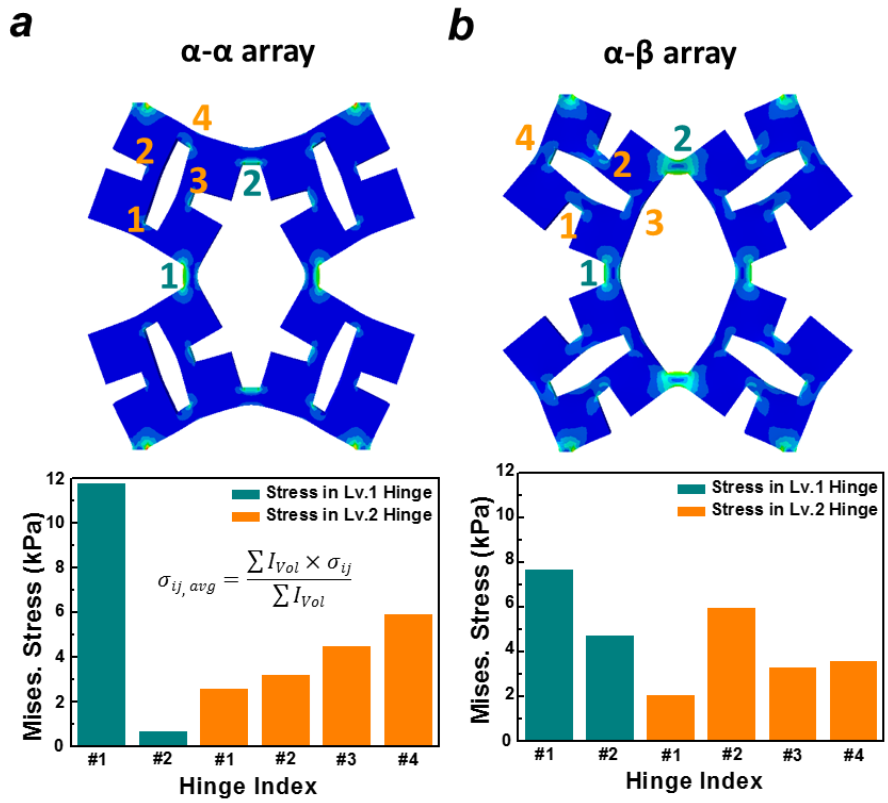

Figure 3.18 Average volume stress of individual hinge of (a) *α-α* array and (b) *α-β* array. *α-β* model was able to distribute the concentrated stress at the hinges of level-1 motif, which would be better in terms of mechanical reliability of hinge.

3.5 Experimental Realization

3.5.1 Mechanical reliability confirmation of hinge

The results in chapter 3.4 confirmed that hierarchical auxetic including a 3D flexible joint hinge is promising architecture for deformable electronics platform. To implement our structure for electronics, the reliability of hinges have to be assured. In chapter 3.2, the motion of hinges was already predicted that stretching, folding and twisting abilities were available to achieve stretching and crumpling for hierarchical auxetic. In order to verify the mechanical reliability of the hinge, numerical analysis was performed at first to predict the magnitude of the strain generated in the hinge during stretching, bending, and twisting as illustrated in **Figure 3.19**. The results presented the principal strain contour according to stretching, bending, and twisting of a single hinge. The hinge was modeled to have a radius of curvature of 4 $inches^{-1}$ to be bent or twisted. Since the hinge was solely deformed without hierarchy structure, mechanical stress could be fully concentrated on a single hinge when the deformation was applied. From the results, maximum strain values were similar among three deformation mode cases; approximately 120% at the edge of the adjacent unit and the hinge, and 60% of the strain generated in the surface of the hinge. Since the individual deformation contained bending, the strain would be decreased as it got closer to the center of the hinge, which would be important to be considered in interconnect integration.

The simple tensile test was performed to convince the reliability of packaging material for hinge. For packaging materials, silicone rubber was applied. **Figure 3.20** represented the stretch test of the hinge. Initially, the hinge rotated until the angle of the adjacent unit

to be 45°, then deformation of the hinge changed to the stretching. The hinge withstood the magnitude of strain over 130 %. Therefore, the mechanical reliability of hinges could be guaranteed. In addition, the stress concentrated on the hinge could be even relieved when hierarchical design would be added. In this case, silicone rubber was considered to be suitable as a packaging material to sustain mechanical reliability in the hinge.

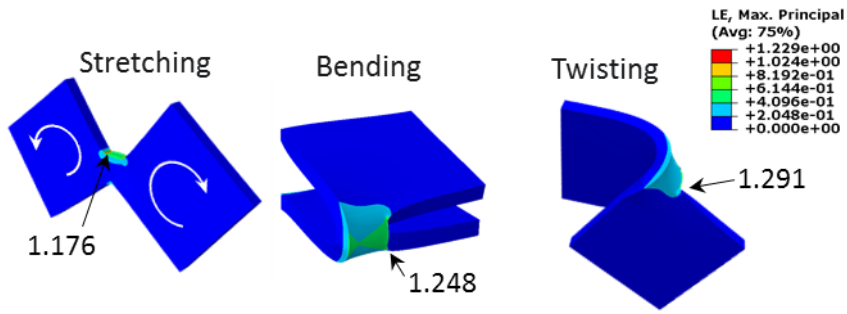

Figure 3.19 Maximum principal strain contour of single hinge under stretching, bending, twisting. Contours indicated that strain mainly concentrated at the hinge, which indicated that the unstressed unit volume could be utilized as active device site.

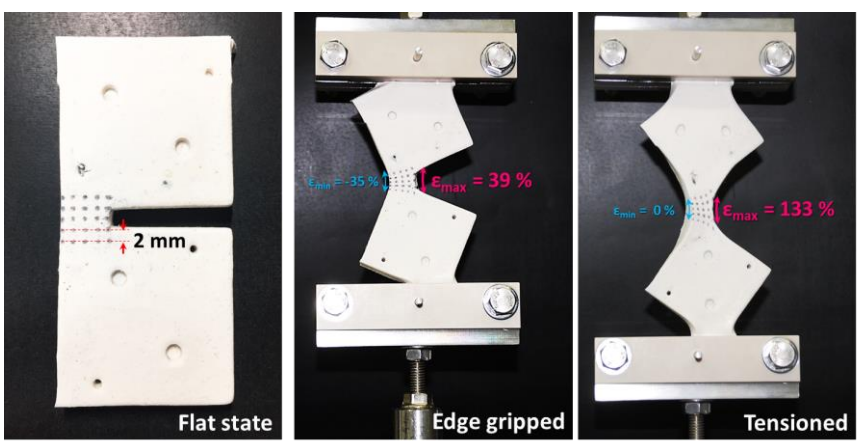

Figure 3.20 Experimental verification of strain endurance of silicon rubber for packaging material. The stretched hinge was mechanically stable even the magnitude of strain reached to 130 %, which were beyond the values obtained from numerical results.

3.5.2 Omni-directionally deformable battery

Through the numerical and experimental verification above, hierarchical auxetic manufactured by silicone rubber had sufficient potential to be used as extreme deformable device platforms without limiting mechanical reliability. To prove our concept, we fabricated omnidirectionally deformable battery based on level-3 hierarchy structure as shown in **Figure 3.7**. If the hierarchical level is too large, the size of the unit becomes smaller than expected, which could make it difficult to package the cell. Therefore, a level-3 single lattice design was chosen.

Figure 3.21 showed the stable performance of fractal cut battery under dynamic deformation. The battery was connected with the movie player, and it was confirmed that the movie player was still operating well while the battery experienced severe stretching and crumpling. From the results, it could be assumed that negligible distortion occurred in the lithium ion cells place on the strain-free unit cell areas, and the entire deformation behavior was dominated by the hinges. The coulomb efficiency of the battery was 99.4 % and the capacity retention of our battery during 100 cycles was estimated to 95 % respectively.

Figure 3.21 Snapshots captured from the video showing the stable operation of the omni-directionally deformable battery at various deformation modes.

3.5.3 Hierarchical auxetic design for thin film application

Recently, a traditional paper art, *Origami* and *Kirigami* technique was applied to the 2-dimensional sheet and was applied to various engineering sites including robotics, flexible electronics, defect chemistry, and so on.[11, 24-27] The researches of fabricating deformable batteries in previous part were actually processed by resin molding, which was quite a thick, bulky structure. In the present part, inspired by *kirigami*, hierarchical auxetic was applied to the polymeric substrate through cut patterning and finally produced expandable and foldable printing battery.

Figure 3.22 tensile deformation of a patterned Polyimide (PI) substrate having a level-2 hierarchy. The fabrication of auxetic pattern was performed by laser cut. Mechanical failure of the patterned PI substrate was occurred at 16 % stretch. The failure site of patterned PI was at the lowest level of the hinge, which well agreed with the simulation results in previous chapter. Though it was a noticeable result that the PI could stretch over 10 % without any failure or permanent deformation, (The yield strain of pristine PI was known to 3 %) it was much less than the ideal hinge condition, which was reported as 70 % for the similar case. The mechanical failure in the PI substrate was actually derived from the crack propagation at the hinge, therefore it was necessary to revise the design of hinge to prevent crack growth to achieve enhanced mechanical property. To solve the problem, T-shape cut pattern was adapted, which could block the notch effect resulted from the sharp cut pattern. In this case, the length of the hinge increase and easier to be buckled in the normal direction. Modified design of hinges was illustrated in **Figure 3.23**.

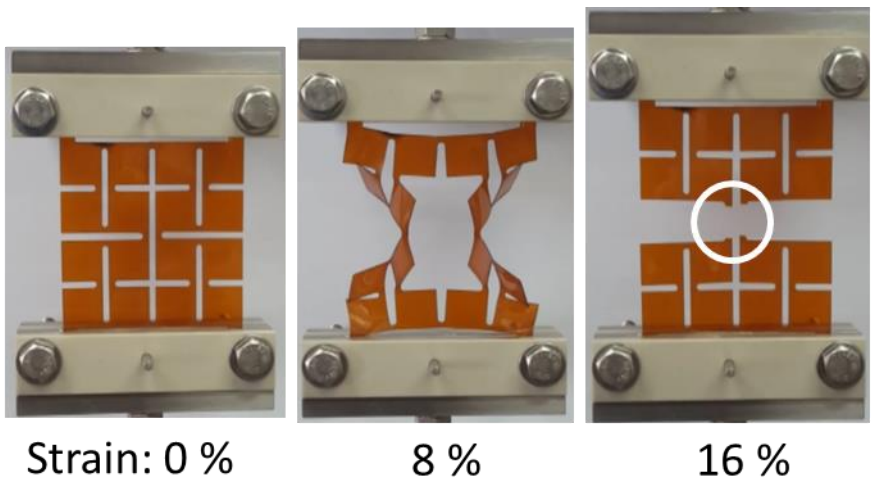

Figure 3.22 Tensile test of level-2 hierarchical auxetic patterned PI substrate. Due to the sharp cut pattern at the hinge, it was vulnerable even under the small stretch.

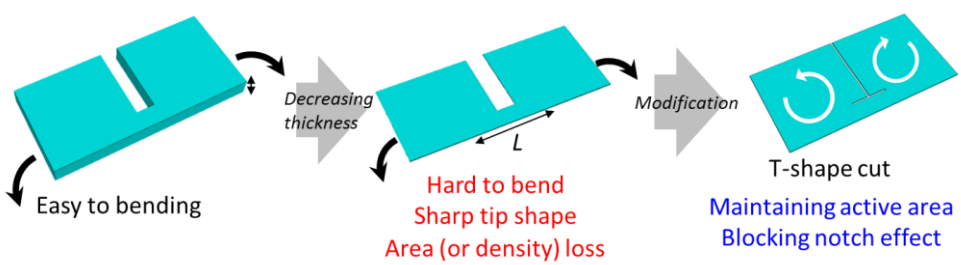

Figure 3.23 Modified design to blunt crack propagation at the hinge.

It was already mentioned in chapter 3.3 that only the graphite current collector was printed on the hinge, where the strain could be concentrated on. When the auxetic expanded or folded, the hinge could undergo bending. Therefore, the mechanical reliability of the graphite current collector should be guaranteed to use hierarchical auxetic as a printing electronics.

From the simulation, the hinge could be bent having 1 mm^{-1} curvature scale, which corresponds to the 2 % strain to graphite film when the thickness of substrate was 50 μm. Sliding bending fatigue test was performed to the graphite/PET substrate system with in-situ resistance measurement of to see whether the mechanical failure could occur under repeated deformation. Sliding bending fatigue test was performed to guarantee the fatigue reliability of graphite electrode. **Figure 3.24** showed the resistance change of graphite conductor during cyclic bending. The film could experience tensile strain when the outward position, and compressive strain vice versa. The resistance change of graphite conductor was less than 1 % for both tensile and compressive case even up to 3,000 cycles, which indicated that the mechanical reliability of current collector at the hinge would be fairly stable.

Based on the screen printed primary type battery was fabricated on the level-1 hierarchy substrate. The output voltage was 1.4 V at the flat state, and the performance did not degrade when the battery was expanded or folded. Based on *kirigami* concept with the revised design at the hinge, the hierarchical auxetic structure could be applicable even to the thin film process.

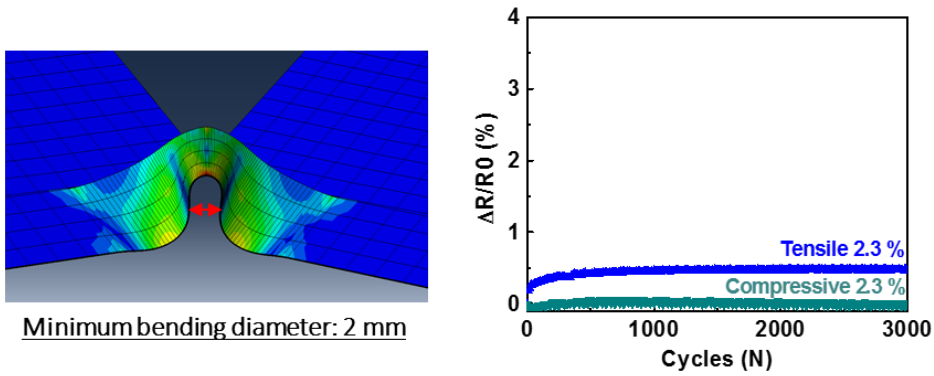

Figure 3.24 (a) Prediction of bending curvature when buckled. (b) Resistance change of graphite current collector during cyclic bending. The resistance changed less than 1 %, which indicated that the strain isolation in hinges cannot affect the degradation of printed battery.

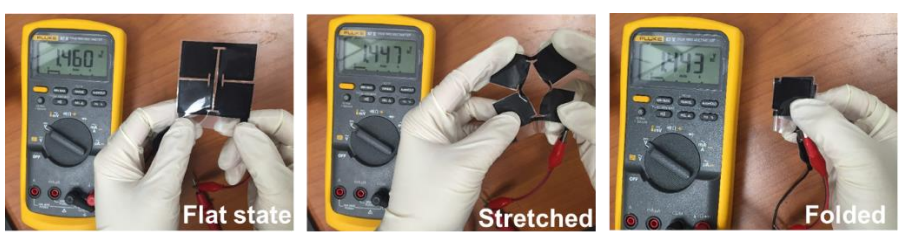

Figure 3.25 Stretching and folding of screen printed level-1 hierarchical auxetic battery.

3.6 Summary

In chapter 3, the effect of the strain isolation characteristics of the hierarchical auxetic under the complex deformation was predicted by FEM simulation and proved by applying it as the extremely deformable battery. In particular, it was first reported that when the rotational hinge was replaced with a soft material, and that it could have unlimited deformation degree of freedom in three dimensions, deviating from the existing view of observing deformation in in-plane only. They could be pulled well based on the excellent expansion characteristics of the auxetics, as well as being easily crumpled based on the porous structure. Especially, it was confirmed that the strain isolation effect selectively occurred only in the hinge under crumpling. This hierarchical auxetic design could be also fabricated as a thin polymer substrate through a cut-based process. In this case, the hierarchical auxetic structure could be applied to a printing electronics by improving the mechanical stability through the modified hinge design which could suppress the crack propagation. From these results, it can be concluded that the hierarchical auxetic is able to be utilized appropriately as a unique structure for flexible devices even adapting various process solutions.

CHAPTER 4

Tunable Elastic Property of Soft Materials by Auxetic Composite and Stretchable Strain Sensor Application

4.1 Introduction

Researches of soft materials are rapidly expanding recently. Soft materials were the materials having low Young's modulus and incompressibility, i.e. they could be easily deformed by external forces in an intuitive sense. Soft materials in the real world included liquids, polymers, rubbers, gels, several biological materials, etc. Based on their mechanical features, soft materials could show interesting physical phenomena that conventional stiff materials did not show or could not solve: e.g. they could show a flexible response to unexpected external factors, while the rigid materials could only show the designed response. Due to their unique mechanical characteristics, soft materials could be applied in wide range of applications. With the growing interest in human-based and biomedical devices, the development of soft-material-based technologies with similar mechanical properties is expanding, for example, soft robots, wearable sensors and actuators, bioscaffolds, flexible and stretchable devices, and so on.

[1, 28-33]

To provide a functional variety of soft materials, researches for controlling the elastic property of soft materials have been actively carried out to fabricate the materials softer, or making functionally graded materials, and reduce the gap in mechanical properties for improving interface reliability.[34] Due to the ease in modulation, controlling the elastic property of soft materials were mainly focused on modulus control by simple synthesis technique.

In addition to Young's modulus, Poisson's ratio is an important parameter to define the elastic response of a material. Poisson's ratio was defined as the negative ratio of transverse strain to axial strain. Though the importance of determining the elastic response of the material, researches of controlling the Poisson's ratio of soft materials was not well-known. Actually, tuning the Poisson's ratio of the material is still a challenging work compared to the control of Young's modulus.

Figure 4.1 showed the elastic property map of various materials, including Young's modulus and Poisson's ratio. The innate elastic properties of a material could be determined from the most microscopic point of view, depending on the type of atomic or intermolecular bonding and bonding strength. Unlike rigid materials, soft materials could withstand the large magnitude of deformation due to the low modulus value. Conventional soft materials had weak secondary bonding among the polymer chains which could result in incompressibility. In other words, the Poisson's ratio of soft materials is nearly close to 0.5, which is the theoretical limit of isotropic materials. Though there were some slight differences, it is suggested that the materials having similar bonds could form a group showing similar elastic properties as illustrated in **Figure 4.1**. Unlike the elastic modulus, Poisson's ratio has no significant variation in the region of the same material group. This indicated that the Poisson's ratio cannot be easily

controlled by simple synthesis method.

To solve the problem, we considered the structural design aspects of materials, not material synthesis. The design of rigid material by stretchable structure through cut pattern, or study of changing Poisson's ratio by using foldable structure, are all studies that could change or improve the mechanical properties of materials through structural design. In particular, auxetic, which is a mechanical metamaterial having negative Poisson's ratio, is known to originate from the specificity of the structure, not from material specific properties. Negative Poisson's ratio means that they could expand in the transverse direction when elongated to the axial direction, while conventional materials shrunk. There are many kinds of structures that form the auxetic behavior such as re-entrant, rotating unit, and chiral. However, even in the structure that forms the same mechanism, Young's modulus and Poisson's ratio could be changed according to the geometric factor. Poisson's ratio of auxetic could be greatly affected by the structure factor; in other words, their elastic property could be tuned by selective designs.

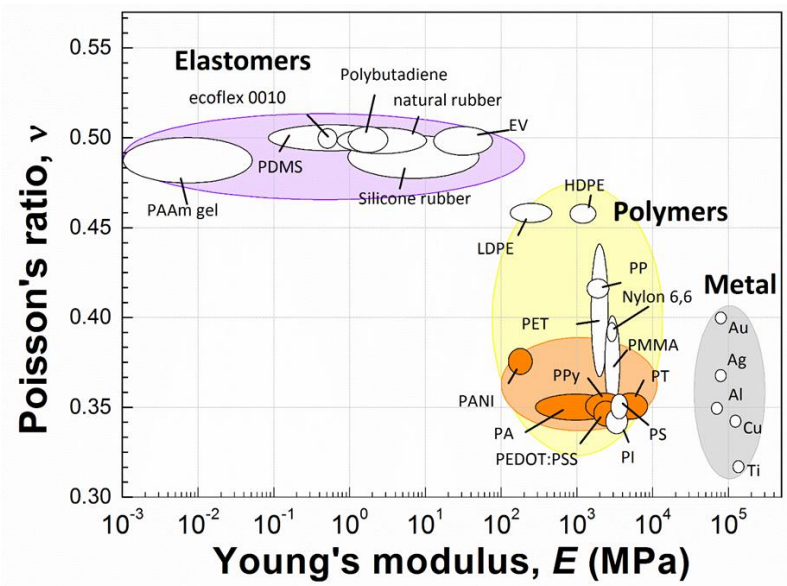

Figure 4.1 Young's modulus and *Poisson*'s ratio of various materials. The *Poisson*'s ratio of conventional soft materials were almost close to 0.5, which would be easier to deform and incompressible.

In the present research, we fabricated a macroscale composite consisting of auxetic to modulate Young's modulus and Poisson's ratio of the soft material. One more important thing is that the soft auxetic composites developed in the present work are a continuum body, which is distinct property from pre-existing auxetic. There had been little research on the existing non-porous auxetic, in particular, only a theoretical modeling of the mechanical behavior of a continuum body with a negative Poisson's ratio was reported.[35] However, studies on whether it actually follows such behavior have not been reported. In this study, we first implemented continuum auxetic of the 3-dimensional plane and analyze actual mechanical behavior. If the Poisson's ratio of soft material could be controlled freely to the range of negative value, it is expected to be applicable to various applications as materials with fascinating features such as high elasticity patches, sensors, robotics materials as well as the unraveled behavior of continuum body. For example, the porous structure of auxetic was not suitable for integrating a wearable device, though they had excellent strength and conformability. By controlling the Poisson's ratio freely, it is possible to maximize or minimize the rate of change of the area according to the tensile, which makes it possible to produce a sensor with superior performance. In addition, it is possible to maintain a perfect surface without wrinkling or buckling on a non-Gaussian plane when having a negative Poisson's ratio, which could be expected to lead to a significant effects in the wearable market. Finally, since some bioscaffolds and biomaterials have a negative Poisson's ratio, they could also play an important role in the understanding and implementation of research in the field of biomaterials.[36] Therefore, the control of the elastic property of the soft material freely will eventually make the soft materials' industry very versatile.

4.2 Experimental procedure

4.2.1 Fabrication of auxetic composite

Schematic of the auxetic composite were illustrated in **Figure 4.2**. The structure in which the auxetic characteristic is maintained had various structures such as re-entrant, rotating unit, chiral, and so on, as aforementioned in chapter 2. Among those various structures, re-entrant auxetic was adopted to be embedded in the soft material. For the present research, soft materials should fill the empty volume of the auxetic structure to fabricate fully solid body. In this case, a large magnitude of local strain could be applied when the auxetic expands, which could be differ depending on the structural type of auxetics. In addition to the local strain effect, Poisson's ratio of re-entrant structure could be tuned in ease by changing the geometric design such as the auxetic unit width and length, and arm width, while other types of auxetics could not. Therefore, the re-entrant structure had advantages for both the ensuring reliability and modulation aspect.

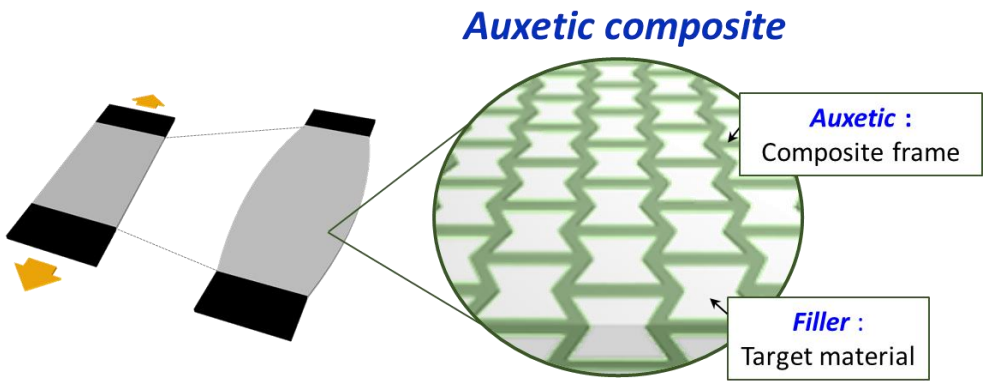

Figure 4.2 Schamtic illustration of auxetic composite. By embedding the re-entrant auxetic into targeted soft material (filler), the Poisson's ratio of filler could become tunable depending on the geometry and material of auxetic, even maintaining non-porous, flat state.

The theoretical minimum value of Poisson's ratio of re-entrant structure could be obtained when the angle between the diagonal and transverse auxetic frame is 60 degrees. To see the largest difference of modulation effect, the angle of a re-entrant structure was fixed at 60 degrees in this researches. In addition to the geometric factors, the Poisson's ratio of the auxetic composite layer could be affected by the intrinsic Young's modulus of the auxetic and filler material. If the modulus of filler is much softer than the auxetic material, the whole composite would follow the elastic behavior of auxetic materials, while the composite would act as a homogeneous material if the modulus of filler and the auxetic material is similar. In order to clearly illustrate the concept of our study, it is necessary to use a filler having a relatively low modulus and auxetic as the material with relatively high Young's modulus.

Figure 4.3 displayed the dimensional and material information of auxetic composite, and fabrication process as **Figure 4.4**. In the present research, we adopted the Polyurethane as a material for an auxetic scaffold, and used Ecoflex™ 0030, as a filling matrix. At first, 0.5 mm-thick TPU sheet was cut into the desired re-entrant structure using a floating cutter to fabricate the auxetic structure. We used commercially provided Polyurethane sheet, and a re-entrant auxetic pattern was achieved through floating cutting method, as illustrated in the first step of **Figure 4.4**. After patterning, the auxetic Polyurethane underwent molding by Ecoflex to have the proper thickness, and finally developed auxetic composite after solidification of Ecoflex.

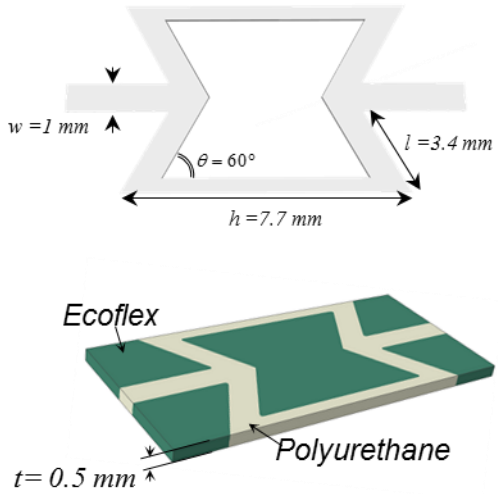

Figure 4.3 (a) Dimension of individual geometric parameter consisting re-entrant auxetic structure. (b) Material information of composite element. For manufacturing auxetic composite, ecoflex was used as a filler material and Polyurethane was used as an auxetic scaffold.

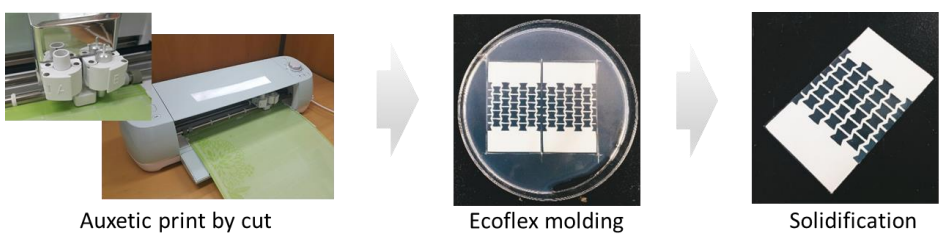

Figure 4.4 Fabrication of process of auxetic composite. Polyurethane sheet was patterned as a re-entrant structure by using floating cutter.

4.2.2 Fabrication and measurement of strain sensor

The fabrication process of auxetic composite based strain sensor was represented in **Figure 4.5**. For the electrode, PEDOT:PSS/Acrlyamide (AAm) organogel was used, which could be stretched up to 300 % even without the conduction change.[30] Strain sensor was fabricated by laminating the PEDOT:PSS organogel electrode upside and downside of the auxetic composite layer. After forming the electrical contact, the PEDOT:PSS gel conductor was covered by Ecoflex to inhibit the drying of organogel. To investigate the strain sensing behavior of fabricated devices, the capacitance of the strain sensors was measured in situ upon stretching until 50 % strain.

The fabricated auxetic strain sensor was stretched to 50 % by INSTRON tensile tester. Parameter analyzer was used for capacitance measurement during stretching.

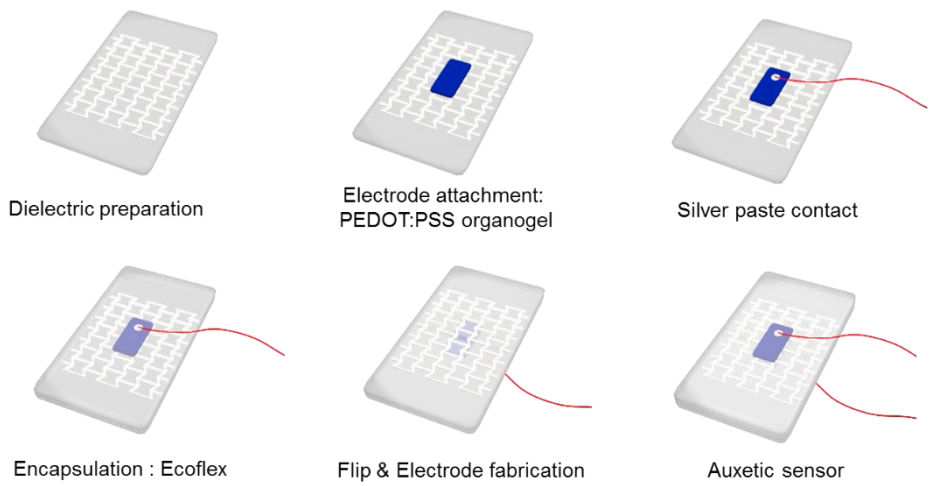

Figure 4.5 Fabrication process of stretchable strain sensor using hybrid auxetic composite as a dielectric layer and PEDOT:PSS organogel as an electrode.

4.3 Tensile behavior of auxetic composite

To figure out the auxetic behavior of our fabricated composite, we elongated both the pristine Ecoflex sheet and auxetic composite sheet, as illustrated in **Figure 4.6**. The elongation of the soft materials reached to 30 %. Large lateral shrinkage of the pristine Ecoflex layer under tension. Unlike the lateral shrinkage of pure Ecoflex, the auxetic embedded layer displayed expansion in a transverse direction when stretched. Poisson's ratio of composite layer was measured using optical microscopy by calculating the ratio of longitudinal and transverse strain from the four reference points, which were placed in the middle of the unit at the center of the tensile specimen. Quantitative result of transverse strain versus axial strain was plotted in **Figure 4.7**. The negative sign of transverse strain indicated that Ecoflex had a positive Poisson's ratio, while a positive sign of transverse strain were observed in auxetic composite. Poisson's ratio of auxetic composite was initially -0.4 and increased as stretch proceeded, which was explained later in detail.

Since the volume of the filler itself did not change during the stretching of composite and the embedded auxetic was 2-dimensional structure, Poisson's ratio in the normal direction was expected to increase more positively as the Poisson's ratio in the xy-plane increased in the negative direction, which would be an important characteristics for applying auxetic composite as a dielectric materials of stretchable strain sensor. Comparison of deformation morphology between conventional soft material and auxetic composite were illustrated in **Figure 4.8**.

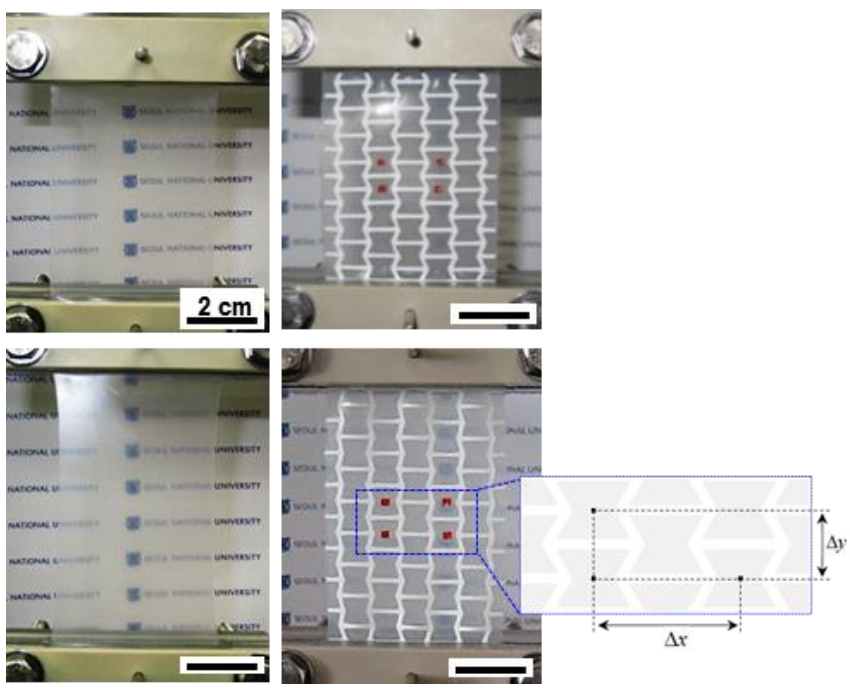

Figure 4.6 Tensile morphology of pristine Ecoflex and auxetic composite. When elongated, lateral shrinkage could be observed for pristine Ecoflex, while lateral expansion was occurred in auxetic composite. The points in auxetic composite was a reference to measure *Poisson*'s ratio.

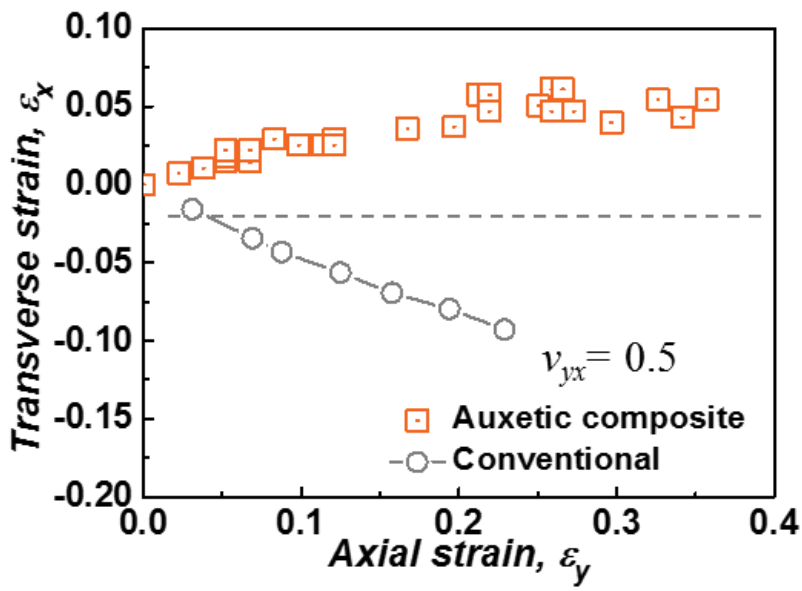

Figure 4.7 Changes in *Poisson*'s ratio during stretch.

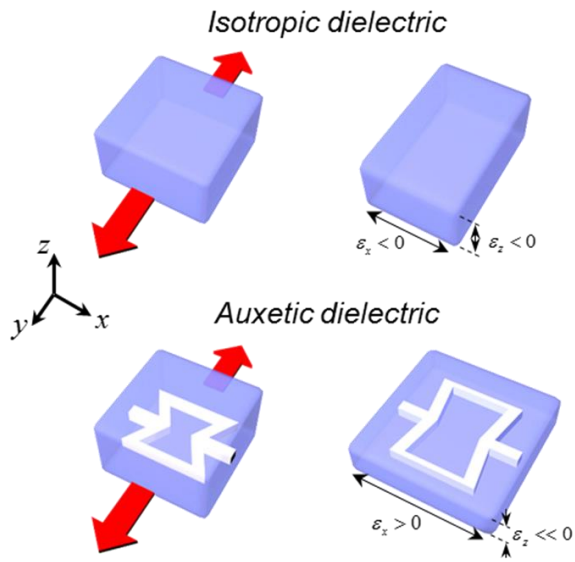

Figure 4.8 Tensile deformation characteristics of isotropic material and auxetic composite material. Due to the negative Poisson's ratio property in xy-plane, the auxetic composite could decrease their thickness more than the conventional isotropic material under same magnitude of stretch.

4.4 Auxetic composite design through FEM

4.4.1 Determination of elastic property of composite element

From the experimental procedure in chapter 4.2, Polyurethane was used for auxetic material and Ecoflex was used as filling material for experimental realization. In addition to that, PDMS was added to composite material elements in this session to consider the dependence of modulus gap between composite elements on the mechanical behavior of composite. To figure out proper mechanical property variables for numerical analysis, a tensile test of each material was performed. The stress-strain relationship of Ecoflex and Polyurethane was presented in **Figure 4.9**.

Ecoflex was known to follow the hyperelastic behavior. In this experiment, less than 200 % of strain would be generated in filling material. Therefore, it would be suitable to fit neo-Hooekan model, which is the simplest model to describe the hyperelastic behavior of elastomer. From the neo-Hookean fitting in Figure 4.9, the C_{10} and D_1 parameters for Ecoflex were 0.068 and 0.007, where C_{10}= G/2 and D1=2/κ. In the same way, the neo-Hookean parameters of PDMS were obtained to be 0.068 and 0.007.

Permanent elongation was occurred in the tensile test of Polyurethane, indicating that they underwent plastic deformation. In this case, the Young's modulus, Poisson's ratio, and yield stress of Polyurethane was obtained to be 15 MPa, 0.49, and 0.94 MPa, respectively.

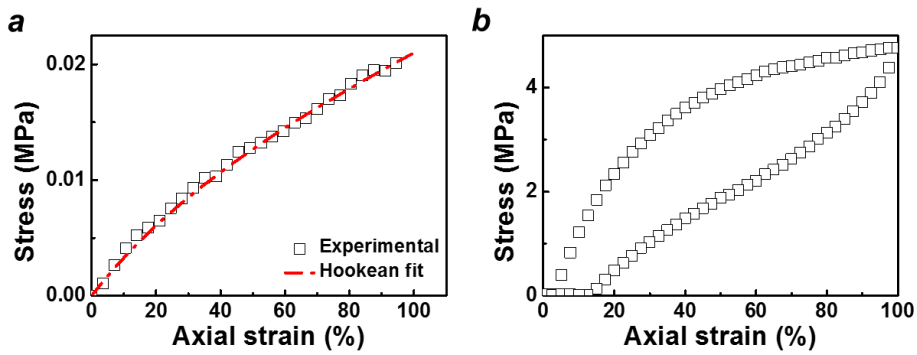

Figure 4.9 Stress-strain behavior of (a) Ecoflex and (b) Polyurethane.

4.4.2 Stretch direction dependence of re-entrant auxetic

The structure of re-entrant auxetic is asymmetric, or the auxetic behavior can depend on the direction of stretch. Before analyzing the auxetic composite, the stretch direction dependence of re-entrant auxetic was firstly considered when the auxetic underwent large magnitude of the stretch.

The re-entrant auxetic is possible to stretch in a vertical direction or horizontal direction. **Figure 4.10** showed the transverse displacement contour of re-entrant auxetic, stretched to either vertical or horizontal direction. When pulled vertically, the transverse rib of the auxetic structure was pulled outward to show the negative Poisson's ratio behavior. In this case, no matter how much auxetic is pulled, the angle between the horizontal rib and the diagonal rib cannot exceed 90°. That is, the auxetic pulled in the vertical direction always is able to show a positive transverse strain. On the other hand, when pulled horizontally, the lateral ribs of the auxetic come out of the re-entrant structure as shown in the Figure 4.10. In other words, auxetic initially behaved negative Poisson's ratio performance but would change to positive Poisson's ratio as stretching proceeded. In fact, transverse strain started to decrease when the tensile strain of auxetic was over 35%, and the Poisson's ratio is also larger than when pulled in the vertical direction, as illustrated in **Figure 4.11**. In this thesis, experiments and calculations were carried out in a direction perpendicular to pulling the auxetic structure to show the auxetic effect more clearly.

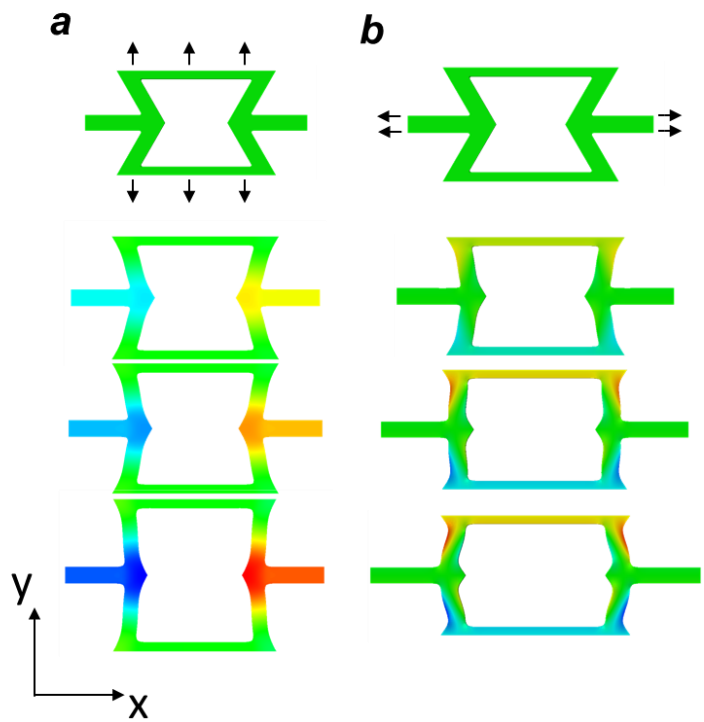

Figure 4.10 Displacement contour of re-entrant auxetic in transverse direction. (a) Vertically stretched auxetic (b) Horizontally stretched auxetic. When auxetic was stretched in horizontal direction, the sign of Poisson's ratio could be changed to be positive when the stretch became severe.

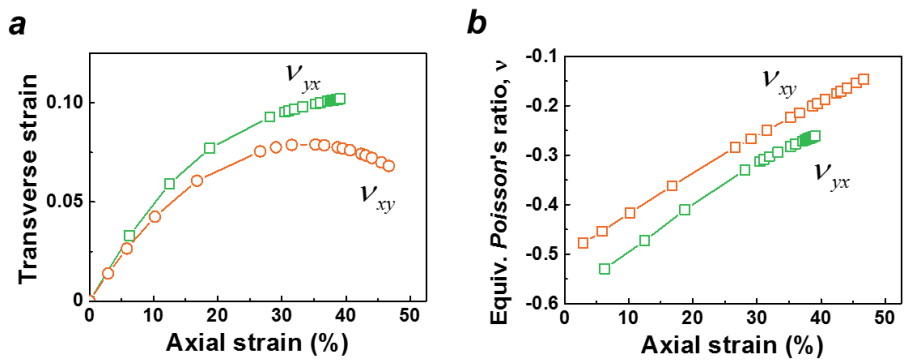

Figure 4.11 (a) Transverse strain and (b) Equivalent Poisson's ratio of re-entrant auxetic when stretched into vertical direction (green line) and horizontal direction (orange line)

4.4.3 Boundary condition for stretch of auxetic composite

Figure 4.12a represented the schematic illustrations of the auxetic composite. The composite had symmetry in x and y axis, therefore the entire model could be decreased to 1/4 with proper boundary condition. The simulations were performed by finite element method (FEM) using ABAQUS. Proper material properties were applied to polyurethane and Ecoflex calculated from chapter 4.4.1. Simulations were performed using the similar scale of a fabricated specimen and representative volume element (RVE) model with periodic boundary condition. Stretching deformation was proceeded by displacement control. The U_1 displacement contour in **Figure 4.12b** indicated that the lateral expansion of auxetic composite was effectively achieved.

Figure 4.13 displayed that Poisson's ratio under tension showed similar results for both the experimental and FEM simulation. Therefore, the boundary conditions applied to simulation was suitable. Poisson's ratio increased from -0.4 to -0.2 depending on the tensile strain. The frame of re-entrant auxetic could show three kinds of hinge motion while expands, including bending, hinging, and stretching concurrently.[18] Therefore, the increase of Poisson's ratio depending on the tension might be related with the elongation of an auxetic material itself in addition to the structural opening. Similar Poisson's ratio value was obtained in both experimental and numerical results.

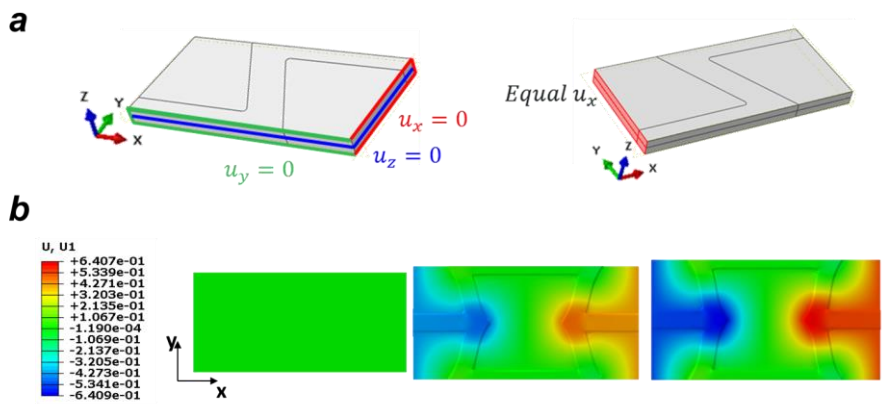

Figure 4.12 (a) Boundary condition of the auxetic composite. Considering the symmetricity, the RVE model could be reduced by a quarter. To provide periodicity, the lateral side of the nodes were fixed to have the similar magnitude of displacement. (b) The U1 displacement contour during stretching. The contour indicated that the auxetic property was achieved by the coming out of the lateral rib.

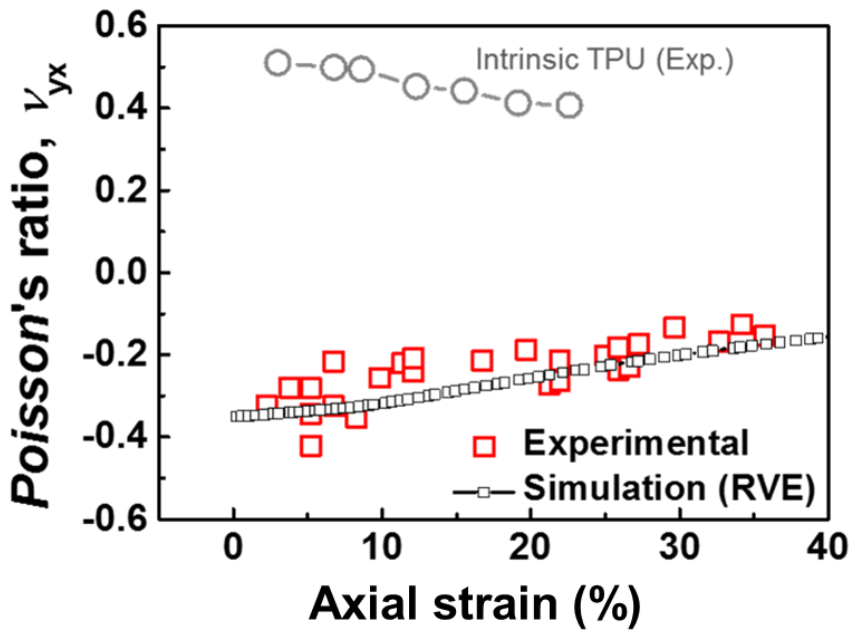

Figure 4.13 Comparison of Poisson's ratio between experiemental and numerical results. The applied boundary conditions were appropriate in that the results were well matched.

Figure 4.14 represented the strain contour of the auxetic composite under stretching. When stretched, the transverse arm of polyurethane auxetic was not stretched because Young's modulus of polyurethane and Ecoflex was about three orders of difference. From the stretching behavior above, deformation in the thickness direction was expected to take place severely in the filling material rather than auxetic structure. In particular, our composite was possible to perform negative Poisson's ratio behavior in the two-dimensional plane since the two-dimensional auxetic structure was embedded, while it could not in the thickness direction. More importantly, thickness had been decreased more severely in the auxetic composite than conventional soft materials at the same tensile level, in order to keep the volume of soft material constant during deformation. This anisotropic deformation behavior is possible to describe the improvement of the sensitivity of capacitive type strain sensor, which would be introduced in a later session. **Figure 4.15** showed the strain distribution along the dash line depicted in Figure 4.14. The maximum ε_{yy} strain localized at the interface of Polyurethane and Ecoflex depicted in the points A and C shown in Figure 4.14, and returned to global level when moved away from the interface. Meanwhile, the strain was mostly generated at the center of the filler material. From this result, the deformation of filler region is expected to change the capacitance dominantly when auxetic composite would be applied to dielectric for capacitive type sensor.

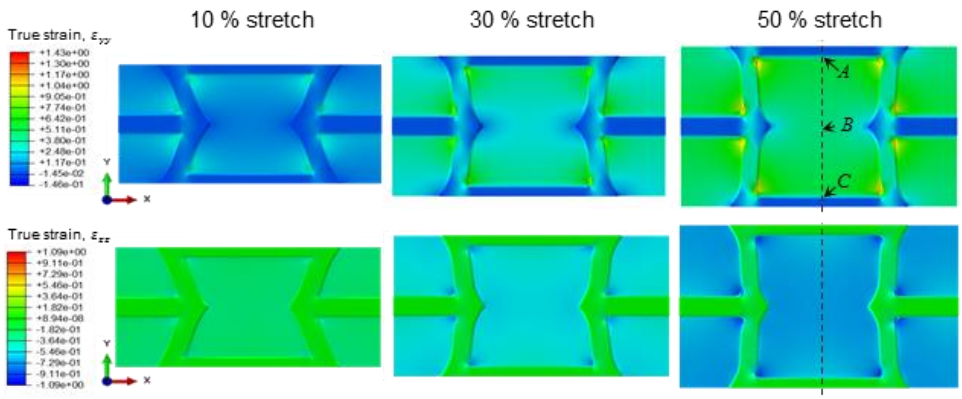

Figure 4.14 Strain contour of auxetic composite during stretch. Upper displayed the strain contour in vertical direction and lower illustrated the strain contour in thickness direction. Strain distribution depicted in dashline were represented in Figure 4.15.

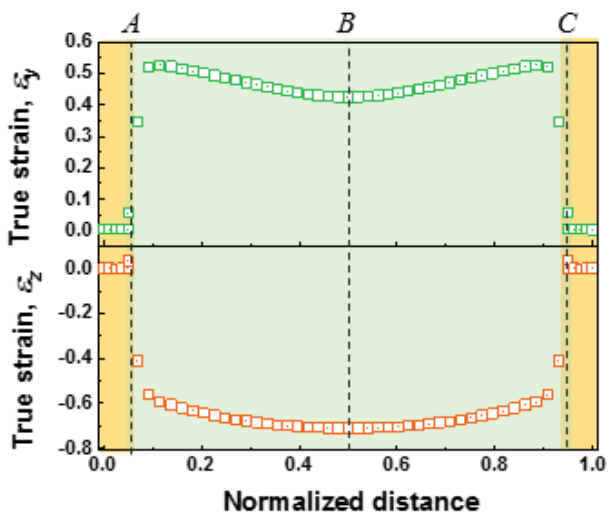

Figure 4.15 Quantified strain distribution in vertical direction of auxetic composite when stretched to 50 %. Deformations were mainly occurred in filling material, and the maximum strain localization could be occurred at the interface of auxetic rib and filling material.

4.4.4 Geometric dependence

Elastic modulus and Poisson's ratio of auxetic composite could be easily tuned on purpose, by selecting a proper composite material and geometric design of the re-entrant structure. In this stage, the dependence of intrinsic modulus of the composite material element and the geometric design of a re-entrant auxetic was figure out through FEM simulation.

Geometric factors of re-entrant auxetic unit were classified into 4 categories excluding the normal thickness. As depicted in **Figure 4.16**, the shape of re-entrant auxetic rib thickness *t*, unit width *w*, and diagonal rib length *h*, and the re-entrant angle θ. In this case, the re-entrant angle was fixed to be 60°, and the dependency on the remaining three geometric factors was analyzed. The dimension of each geometric factor of re-entrant auxetic was presented in **Table 4.1**. To amplify the auxetic property, the material property of composite here was chosen to be similar to the experimental proof, Polyurethane for auxetic and Ecoflex for filling material.

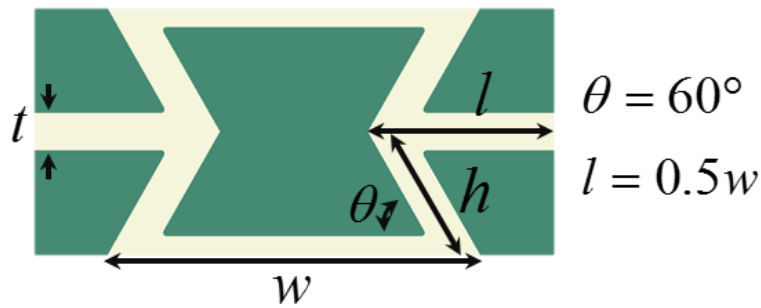

Figure 4.16 RVE model of auxetic composite indicating the geometric parameters. In the present research, the angle was fixed to 60° and three design variables, rib thickness *t*, unit width *w*, and diagonal rib length *h* was considered to control the elastic property of auxetic composite.

Table 4.1 Dimension of geometric parameters applied for FEM simulation

	Rib thickness, *t* (mm)	Unit width, *w* (mm)	Diagonal length, *h* (mm)
#1	0.7	10.74	8.08
#2	1	10.74	8.08
#3	1.3	10.74	8.08
#4	1	8.82	8.08
#5	1	6.9	8.08
#6	1	10.74	6.93
#7	1	10.74	3.77

Geometric dependence of re-entrant auxetic structure on the Poisson's ratio of composite were calculated. The dependence on the auxetic rib width (**Figure 4.17**), auxetic unit width (**Figure 4.18**) and the diagonal length of auxetic rib (**Figure 4.19**). Since the constituent material of auxetic had a Young's modulus greater than three orders of magnitude higher than that of the filling material, the difference in the stress behavior between the auxetic structure and the auxetic material is considered to be negligible. When the auxetic composite is stretched, the transverse strain gradually saturated and Poisson's ratio increased to positive value. This result indicate that our auxetic composite was not a homogeneous system, and the saturation behavior might be expected to be related with the structural factor of re-entrant. Previous literature suggested that the flexible re-entrant auxetic is possible to behave in three motions: bending, hinging, and stretching of the diagonal rib. After all of the auxetic was structually expanded, the stretching of the auxetic material itself may be expected to occur. Auxetic design proposed in this study, which have 60 degrees of re-entrant angle, is able to achieve a structural expansion of up to about 15%, assuming that the auxetic behaves only in the hinging motion. After that, stretching by the material which constitutes the auxetic occurs. In fact, Poisson's ratio increased suddenly to positive value approximately at 11% of the stretch. The point at which the Poisson's ratio started to increase suddenly is expected to be delayed when the re-entrant angle would be designed to be narrower. The fact that Poisson's ratio is not constant according to the stretch should be considered when designing our customized auxetic materials on purpose.

Partial volume of stiff polyurethane increased in the auxetic composite as the thickness of auxetic rib increased. Therefore, the equivalent Young's modulus of our composite increased accordingly. In contrast to that, the Poisson's ratio of the auxetic composite was growing positive when the thickness of auxetic rib increased. When the

re-entrant structure opened, the diagonal rib of re-entrant structure could be stretched simultaneously in addition to the hinging motion. During the stretching, the lateral shrinkage of diagonal rib occurred, which could result in the motion increasing Poisson's ratio positively. Therefore, increase in rib thickness could enhance the lateral shrinkage and finally the Poisson's ratio of auxetic composite increased.

As the width of auxetic was reduced, it seemed that Young's modulus increased rapidly from a certain moment. Since Young's modulus of the composite was determined solely by the force required to unfold the auxetic hinge and the force required to stretch the diagonal rib of the auxetic, Young's modulus can be expected to change very little if the width of the auxetic was greater than a certain magnitude. However, if the width of the auxetic was too narrow, the strain could be severely concentrated in the filler filling between them. As a result, Young's modulus increased sharply when the width of auxetic unit decreased severe. Therefore, even if the width of the auxetic decreased linearly, it could be seen that Young's modulus increased sharply at any moment rather than linearly. On the other hand, as the width decreased, Poisson's ratio gradually decreases to a negative value. The decrease in Poisson's ratio was due to the decrease of the initial length of width, which attributed to a larger strain value although the lateral displacement was similar in each condition.

Finally, when the height of auxetic decreased, Young's modulus of the whole composite did not change significantly. This could be attributed to the fact that the hinging behavior and the stretching behavior of the auxetic, which affected Young's modulus at the time of composite stretching, were not affected as well as the previous width control. However, when the height of auxetic became extremely small, it would be expected that the strain would be largely generated in a local area similar to the unit width case. As the height decreased, the Poisson's ratio increased, which was due to the

decrease of initial length of height, which attributed to a larger strain value similar to the width dependence case.

Figure 4.20 showed Young's modulus and Poisson's ratio of the composite as a function of the geometric factor of the re-entrant auxetic structure calculated from **Figure 4.17** to **4.19**. In spite of using the same material, it was confirmed that the Young's modulus and Poisson's ratio of the whole composite were able to be changed to a large ratio by adjusting the geometric factor of auxetic. Especially, although the filler filled the vacant area of auxetic, the Poisson's ratio still maintained a negative value.

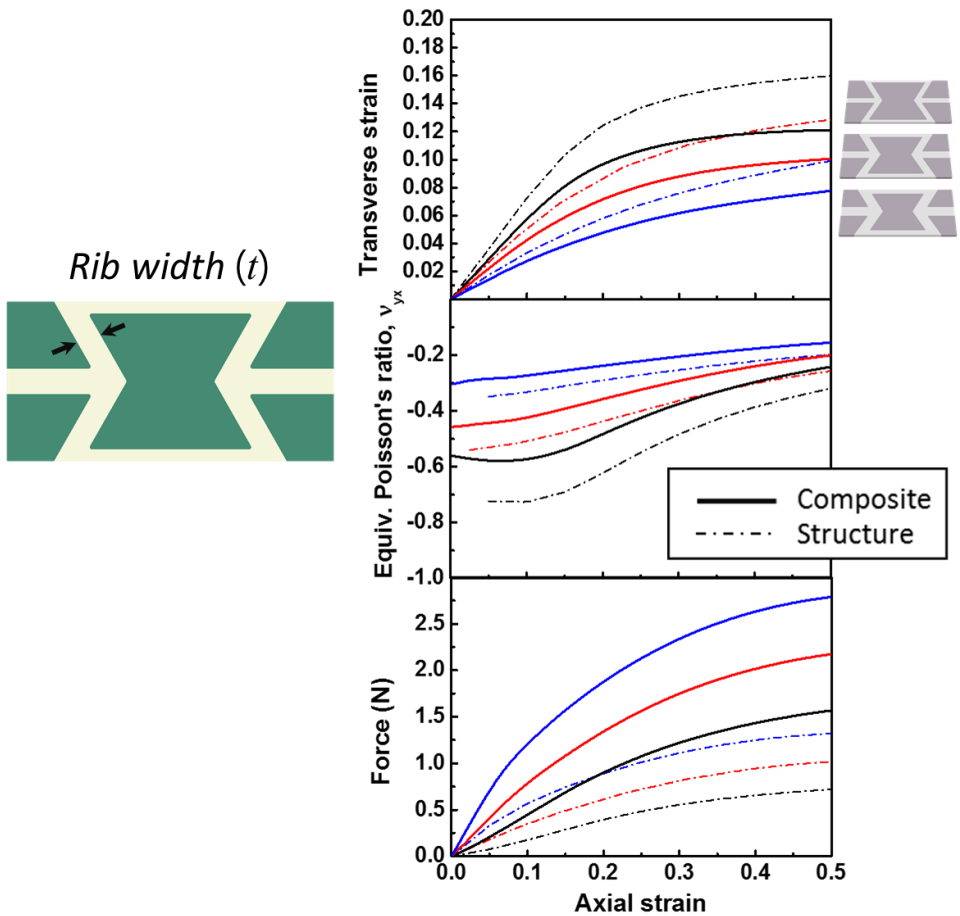

Figure 4.17 Rib width dependence of re-entrant auxetic structure on the transverse strain, Poisson's ratio and reactive force of composite.

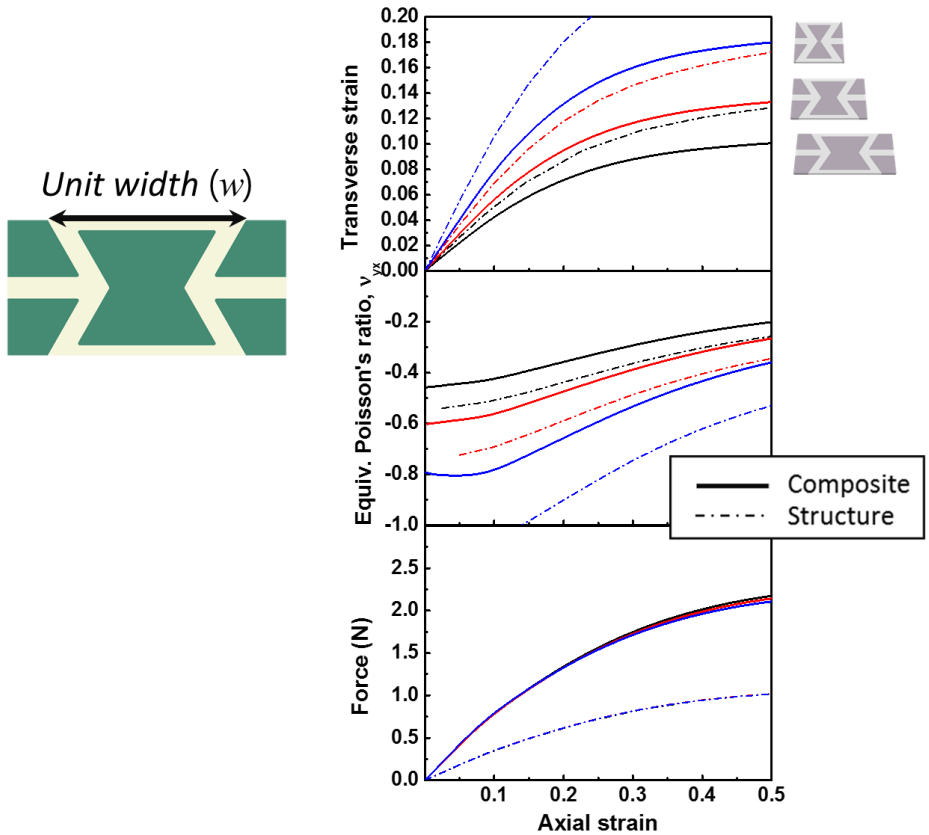

Figure 4.18 Unit width dependence of re-entrant auxetic structure on the transverse strain, Poisson's ratio and reactive force of composite.

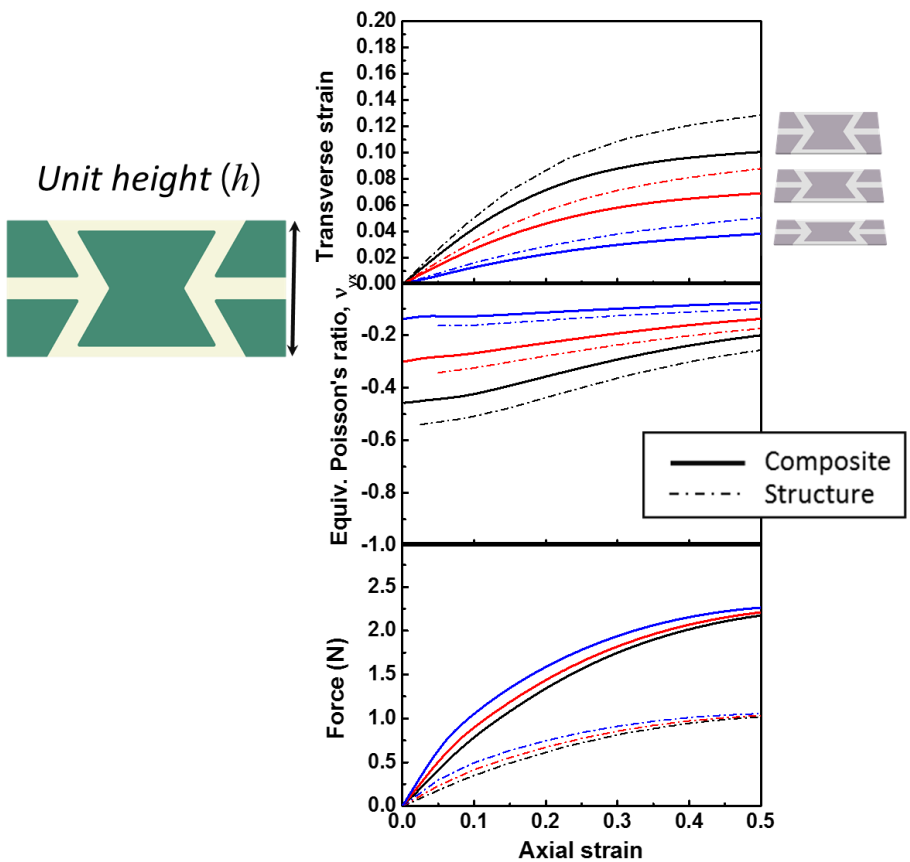

Figure 4.19 Unit height dependence of re-entrant auxetic structure on the transverse strain, Poisson's ratio and reactive force of composite.

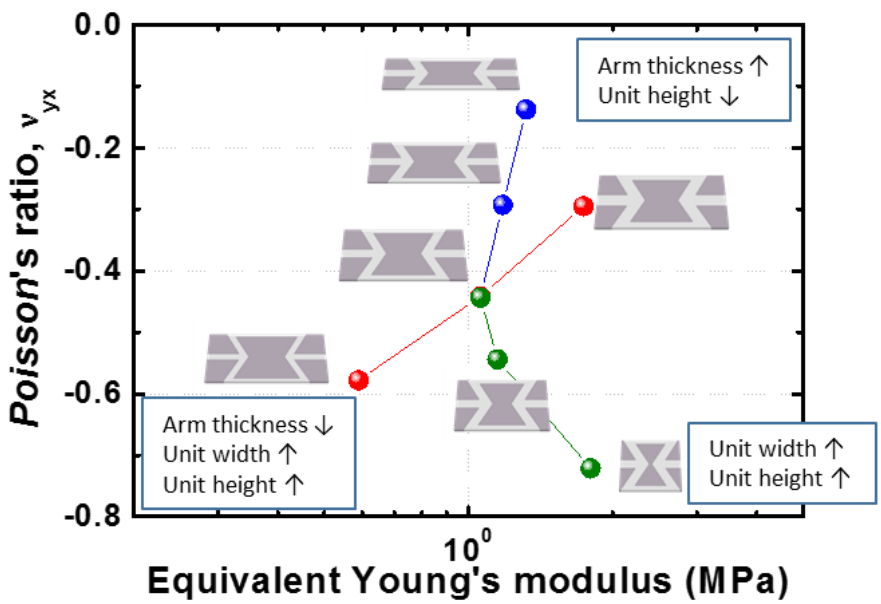

Figure 4.20 Equivalent Young's modulus and Poisson's ratio of auxetic composite varying auxetic geometry, using auxetic as a Polyurethane and filler as an Ecoflex.

4.4.5 Material dependence

In this stage, the dependence of intrinsic modulus of the composite material element and the geometric design of re-entrant auxetic was figure out through FEM simulation. For candidates of composite materials, we additionally included PDMS in addition to the Ecoflex and polyurethane, which were already aforementioned in Figure 4.6 as an experimental proof. The geometric variance was equally applied to a different material property.

When the modulus gap between the auxetic material and filler material decreased, equivalent Poisson's ratio of composite increased, or the composite got closer to the homogenous material. Therefore, the geometric dependence of re-entrant structure could be faded and even show no effect when the modulus gap between the materials was less than 1 order magnitude, as illustrated in **Figure 4.19**. Elastic modulus and Poisson's ratio of auxetic composite could be easily tuned on purpose, by selecting a proper composite material and geometric design of the re-entrant structure.

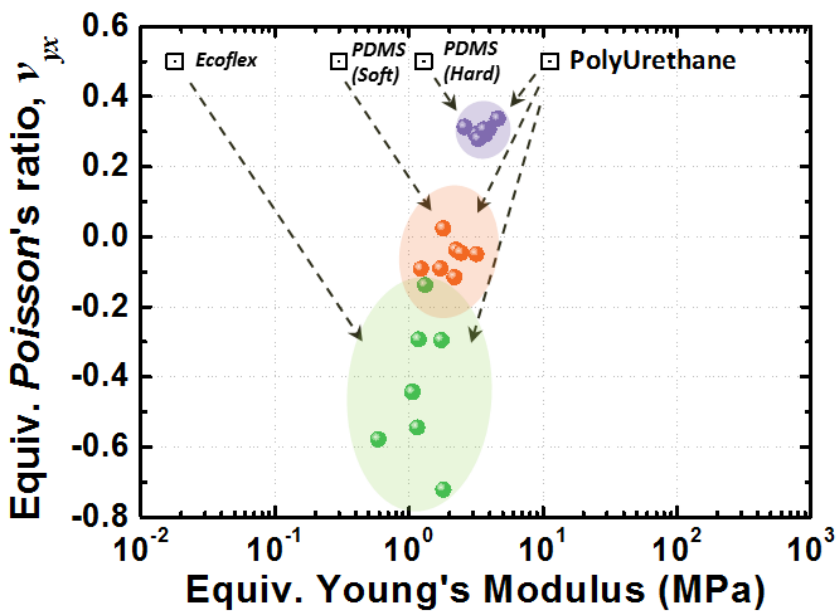

Figure 4.21 Composite material dependence on the Poisson's ratio property of auxetic. When the modulus gap between composite elements decreased, the dependence of geometric factor would be less effective on the Poisson's ratio of composite.

4.4.6 Thickness dependence of auxetic composite

In this chapter, the dependence of thickness on the mechanical behavior of auxetic composite was analyzed. Not only the own thickness of auxetic composite, a method to decrease local strain concentration at the interface of auxetic and filling material was suggested by adapting soft cover layer.

Figure 4.20a showed the thickness dependence on the Poisson's ratio behavior of auxetic composite. Poisson's ratio behavior seldom changed though the thickness decreased. From the strain contour of normal thickness direction in **Figure 4.20b**, it was suggested that the local strain concentration would be more severe as thickness decreased.

In fact, the strain localization could induce mechanical reliability issues when subjected to soft electronics system. The auxetic composite could be utilized as soft substrate material with excellent conformal property and stretchability. However, the local strain concentration was possible to induce mechanical failure between the film and substrate interface. **Figure 4.21** was the strain contour of the auxetic composite with different geometry. Due to the mechanical gap and geometric factor, local strain concentration could easily occur. To solve the problem, soft cover layer was introduced to reduce the strain localization at the filling material.

Figure 4.22 represented the distribution of the longitudinal strain field according to the cover thickness of filler. Cover layer had the same mechanical property with filling material. In the absence of a cover, elongation of auxetic in the longitudinal direction severely occurred. The local strain gap between the auxetic and filling material gradually decreased when the thickness of cover layer was equal to auxetic composite layer. When

the thickness of the filler cover became larger than the auxetic layer, the longitudinal strain of the filler cover immediately above the auxetic increased, which might be the opposite action to the thinner cover layer case. Therefore, it is effective to reduce the local strain gap by fabricating the thickness of the filler cover and auxetic layer as equal as possible the thickness of the filler cover and auxetic layer is effective in reducing the local strain gap, which may contribute to the prevention of local failure of the thin film on the substrate. Because the cover layer was chosen to have the same material as filler, Poisson's ratio and Young's modulus did not change a lot compared with the no cover case, as illustrated in **Figure 4.23**.

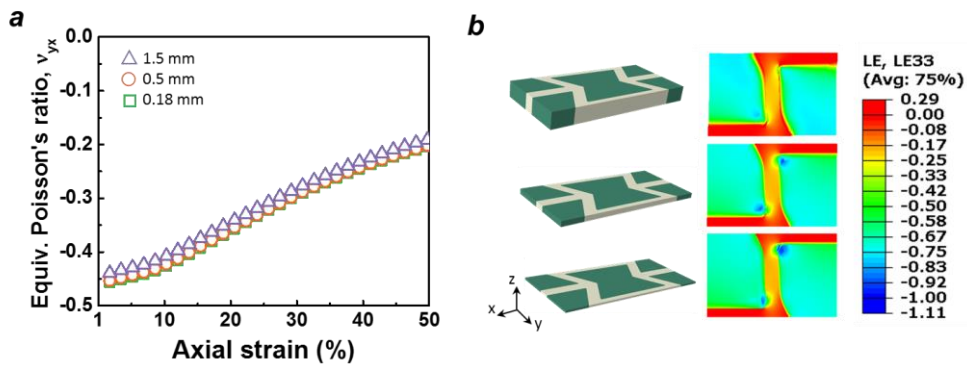

Figure 4.22 (a) Thickness dependence of auxetic composite on Poisson's ratio. (b) Normal strain contour depending on the thickness.

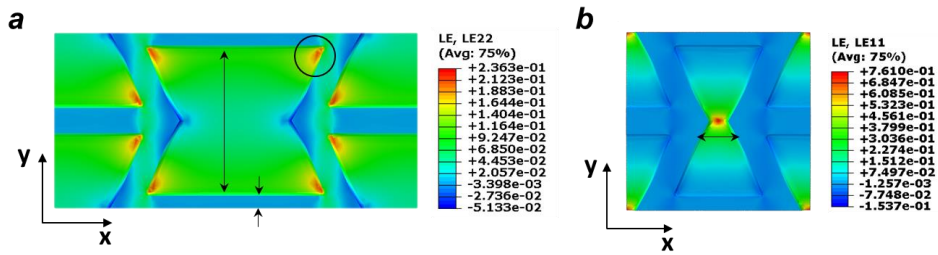

Figure 4.23 (a) y-directional strain contour of auxetic composite. (b) x-directional strain contour of auxetic composite having small unit width. The local strain concentration occurred due to the mechanical gap between auxetic and filling material, which could induce reliability problem when applied to soft substrate.

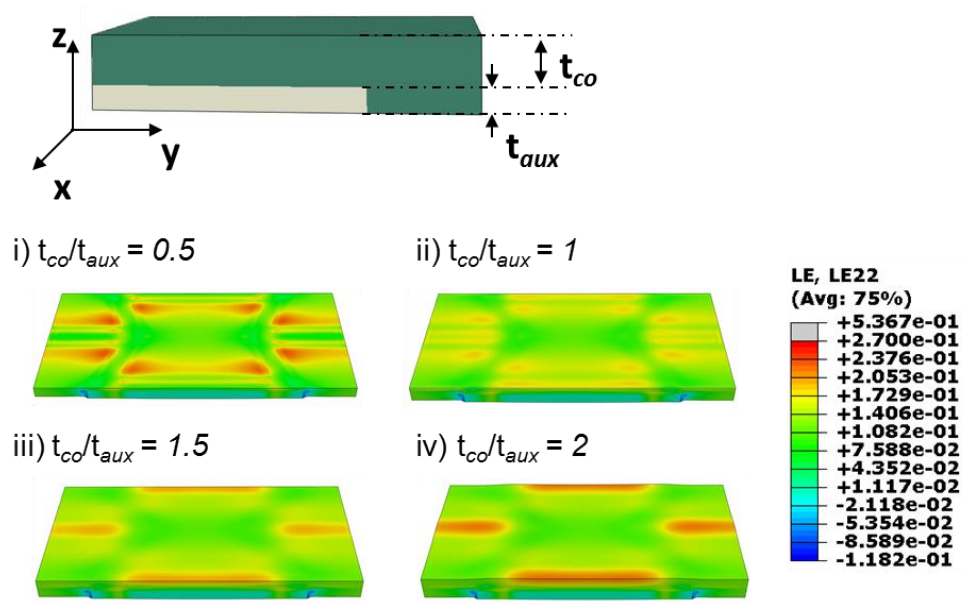

Figure 4.24 Y-directional strain contour of auxetic composite having soft coverlayer. When the thickness of cover was equal to the auxetic composite, the deviation of local strain could be minimized.

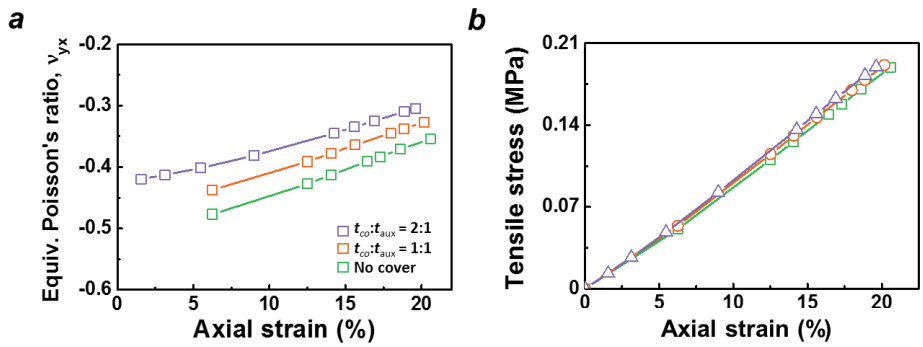

Figure 4.25 (a) Poisson's ratio and (b) Stress behavior of auxetic composite having cover layer.

4.5 Hybrid auxetic composite for capacitive strain sensor

It had already been discussed that the auxetic composite was not actually a 3-dimensional isotropic. Rather, it showed a 2-dimensional semi-auxetic property in xy-plane. Because of the volumetric conservation, the thickness of filling material could be decreased even more when compared to the homogeneous filling material without auxetic embedment under the same magnitude of a stretch, illustrated in **Figure 4.8**. The anisotropic deformation characteristic of the auxetic composite would be expected to improve the performance of capacitive type stretchable strain sensor. The mechanism of capacitive type strain sensor was already aforementioned in chapter 2, that the geometric change such as an area and thickness of dielectric of the soft dielectric material could reflect the change capacitance during stretching, therefore able to quantify the magnitude of the strain from the degree of capacitance change. The advantage of the capacitive type stretchable strain sensor was that the stretching ratio and capacitance change have a linear relationship, indicating that it did not require additional calibration to measure the strain. Though the advantages, the gauge factor, which is a performance parameter of the strain sensor, of the capacitive type strain sensor limited to 1.[37, 38] In this chapter, improving the gauge factor of stretchable strain sensor was investigated by applying the auxetic composite as a dielectric.

4.5.1 Performance of auxetic strain sensor

Three kinds of stretchable sensors were compared. One was the sensor with pristine dielectric, another was using the auxetic dielectric with a small electrode, and the other was using the auxetic dielectric with large electrode. Normalized capacitance change was a lot increased for the case of the auxetic composite as a dielectric material, as illustrated in **Figure 4.24**. The gauge factor of a sensor using pristine elastomer dielectric was measured to be 1 as expected. The sensor applying the auxetic composite was calculated to be 3.2 for small electrode and 2.26 for large electrode, which was better than using the conventional isotropic dielectric material. In addition to the improvement of gauge factor, the relationship between capacitance change and stretch was still linear. The difference between the electrode sizes indicated that the auxetic effect was dominant in the central region of the sheet, which came from the boundary condition of stretch in the grip at the side edge.

The suggested improvement mechanism of gauge factor of auxetic composite could be induced by two geometric factors, one was the area increase of the auxetic due to the negative *Poisson*'s ratio effect, and the other factor was the increase of thickness decrement of filling material. Analyzing which geometric factor would be more dominant to control the gauge factor would be described in chapter 4.5.2 with numerical modeling.

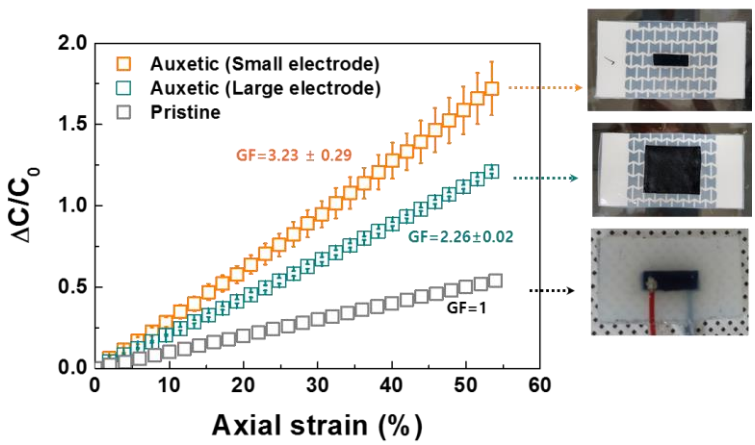

Figure 4.26 Capacitance change versus axial strain using various dielectric.

4.5.2 Capacitance calculation from FEM

Capacitance calculation was performed from the measurement of area and thickness of the auxetic composite. The auxetic composite was composed of an auxetic part and filling material part. For capacitance calculation perspective, those two materials were connected in parallel, therefore the total capacitance of auxetic composite would be:

$$C_{tot} = C_{fill} + C_{aux} = \varepsilon_0 \varepsilon_{r,\,fill} \frac{A_{fill}}{d_{fill}} + \varepsilon_0 \varepsilon_{r,aux} \frac{A_{aux}}{d_{aux}} \qquad \text{(Eq. 4.1)}$$

Where C_{fill} and C_{aux} were the capacitance of filling material and auxetic. In the case of this experiment, Ecoflex was used as a filling material and polyurethane as an auxetic material. Substituting ε_r=3.5 for polyurethane and 2.5 for Ecoflex, the capacitance change could be quantitatively calculated.

From the discussion above, the simulation and experimental results of the normalized capacitance change versus stretch were plotted together. Both the increase in area and the decrease in thickness could contribute to increasing the rate of capacitance change. To investigate which of the two factors had a greater effect on the capacitance change, the capacitance was additionally calculated assuming a boundary condition in which the auxetic composite changed their area only without thickness change.

The gauge factor was about 1.21 when the areal change was considered only, which was not a large difference compared with a conventional elastomeric dielectric. Therefore, the shrinkage in the thickness direction due to the deformation greatly affected the capacitance change. In the case of the capacitance calculated considering

both the areal and thickness change, the gauge factor was about 3.21, which was similar to the experimental measurement value. This result was significant in that it surpassed more than 1 of gauge factor that was difficult to approach with conventional elastomeric dielectrics.

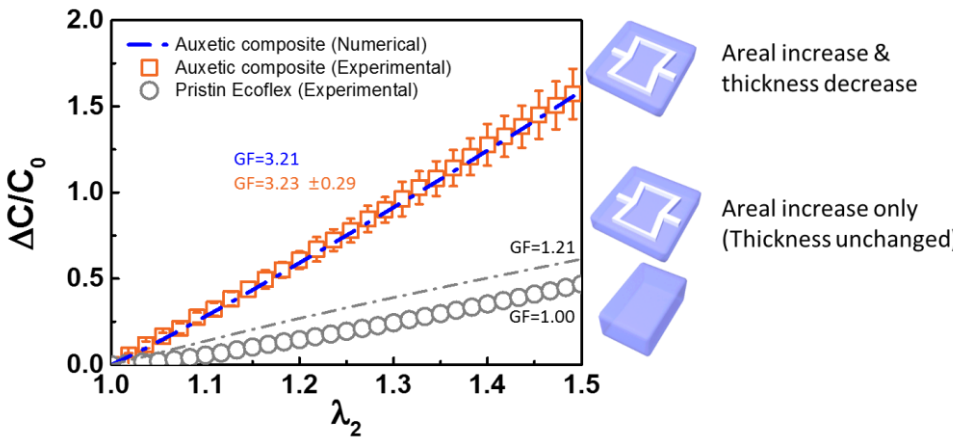

Figure 4.27 Normalized capacitance calculation of auxetic composite from simulation result. The gray line corresponded to the pristine isotropic dielectric. Gauge factor of auxetic composite was calculated as 3.21.

4.5.3 Analytic model for predicting gauge factor

The capacitance change of composite could be approximated as:

$$\Delta C / C_0 = \frac{\Delta C_{fill} + \Delta C_{aux}}{C_{fill,0} + C_{aux,0}} \quad \text{(Eq. 4.2)}$$

Where $C_{fill,0}$ and $C_{aux,0}$ were the initial capacitance of individual filler and auxetic portion.

Since the thickness change would occur dominantly in filler rather than auxetic, the normalized capacitance change could be made in filler. Assuming $\Delta C_{aux} = 0$, then the Eq. 4.1 would become,

$$\Delta C / C_0 = \frac{\Delta C_{fill}}{C_{fill,0} + C_{aux,0}} = \frac{C_{fill} - C_{fill,0}}{C_{fill,0} + C_{aux,0}} \quad \text{(Eq. 4.3)}$$

The capacitance of the filler after the deformation could be expressed as the initial capacitance multiplied by the stretch ratio of individual axis, therefore

$$\Delta C / C_0 = \frac{C_{fill,0} \frac{(1+\lambda_1)(1+\lambda_2)}{(1+\lambda_3)} - C_{fill,0}}{C_{fill,0} + C_{aux,0}} = \frac{\frac{(1+\lambda_1)(1+\lambda_2)}{(1+\lambda_3)} - 1}{1 + C_{aux,0} / C_{fill,0}} \quad \text{(Eq. 4.4)}$$

Gauge factor could be calculated by the ratio of the normalized capacitance change to stretch. Differentiated the Eq. 4.3 with the stretch was followed by

$$\frac{\partial(\Delta C/C_0)}{\partial\lambda} = \frac{1}{1+C_{aux,0}/C_{fill,0}}[\frac{\partial}{\partial\lambda}(\frac{(1+\lambda_1)(1+\lambda_2)}{(1+\lambda_3)})] \qquad \text{(Eq. 4.5)}$$

Since $C_{aux,0} / C_{full,0} = (\varepsilon_{r,aux} / \varepsilon_{r,fill}) \cdot (A_{0,aux} / A_{0,fill})$ where $\varepsilon_{r,aux}$ and $\varepsilon_{r,fill}$ was a relative permittivity of auxetic and filler materials,

,

$$\frac{\partial(\Delta C/C_0)}{\partial\lambda} = \frac{1}{1+\left(\frac{\varepsilon_{r,aux}}{\varepsilon_{r,\,fill}}\right)\left(\frac{A_{0,aux}}{A_{0,\,fill}}\right)}[\frac{\partial}{\partial\lambda}(\frac{(1+\lambda_1)(1+\lambda_2)}{(1+\lambda_3)})] \qquad \text{(Eq. 4.6)}$$

Substituting $\lambda_1 = \nu_{yx}\lambda_2$ and $\lambda_3 = \nu_{yz}\lambda_2$,

$$\frac{\partial(\Delta C/C_0)}{\partial\lambda} = \frac{1}{1+\left(\frac{\varepsilon_{r,aux}}{\varepsilon_{r,\,fill}}\right)\left(\frac{A_{0,aux}}{A_{0,\,fill}}\right)}[\frac{\partial}{\partial\lambda}(\frac{(1-\nu_{yx}\lambda_2)(1+\lambda_2)}{(1-\nu_{yz}\lambda_2)})] \qquad \text{(Eq. 4.7)}$$

From Eq. 4.5 and 4.6, parameters that could affect the gauge factor of the auxetic composite could be divided into three part: the relative permittivity ratio of auxetic and filler material, the in-plane areal ratio of auxetic and filler, and the *Poisson*'s ratio ν_{yx} and ν_{yz}.

If the geometric factor of the composite would be similar, the permittivity dependence on gauge factor of auxetic composite could be fitted as **Figure 4.26**. Realistically, it would be difficult to improve the gauge factor greatly by the difference in permittivity.

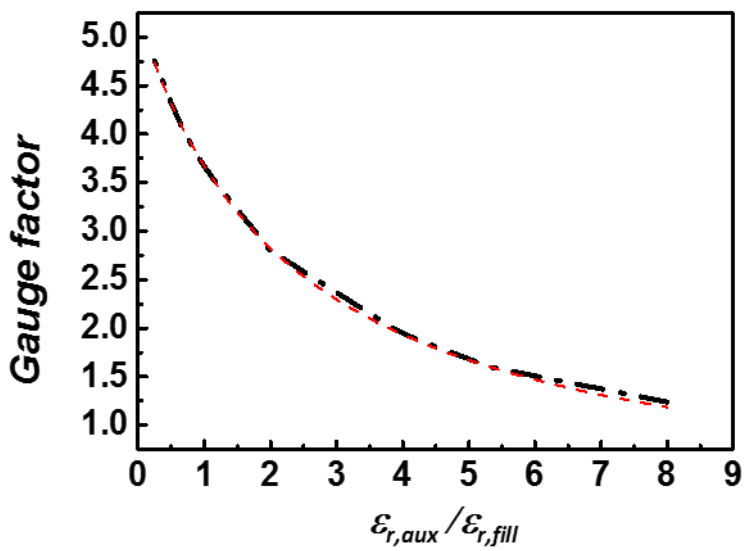

Figure 4.28 Permittivity dependence on the gauge factor of auxetic composite strain sensor. The black line was the simulational results.

Considering the geometric design of auxetic and electrode design, the gauge factor of stretch sensor could be enhanced more. From the previous chapter, we analyzed the geometric dependence of re-entrant auxetic on the Poisson's ratio. Based on the results, the normalized capacitance change was plotted in **Figure 4.27** with a variable geometric design which was already considered in the previous chapter.

In addition to the auxetic geometry, the gauge factor could be improved by considering the coverage region of the electrode. If assuming the electrode only covered the filling region of our auxetic dielectric material, it is unnecessary to consider the capacitance of the auxetic portion anymore, which did not affect the change in capacitance during stretching. **Figure 4.28a** and **Figure 4.28b** showed the normalized capacitance change of same auxetic geometry but was assumed that the electrode covered filling material only in Figure 4.28b. In this case, the gauge factor covering only filling material region could be improved 1.5 times more than covering the whole area of auxetic. From the design consideration, the gauge factor could be enhanced to 7~8 even using the same material. Therefore, proper design consideration with material factor is expected to provide the high sensitivity stretchable strain sensor which was unimaginable in the previous studies.

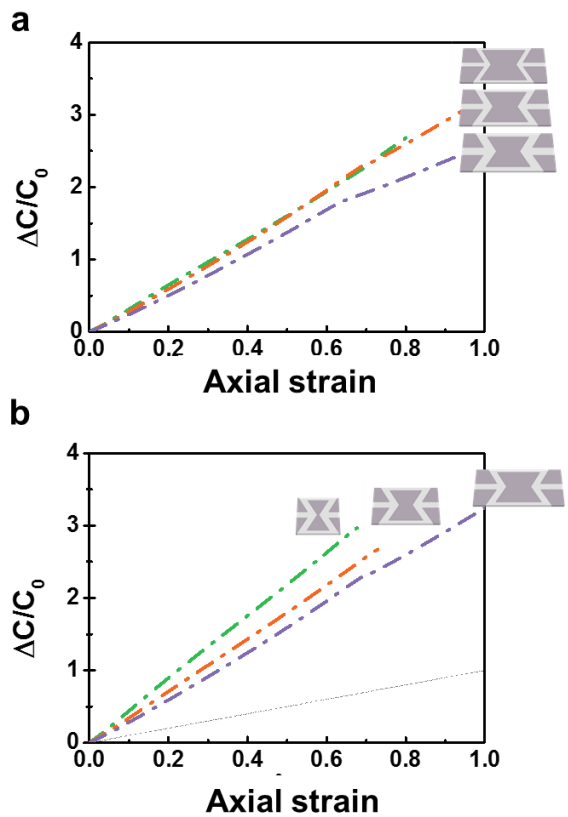

Figure 4.29 Geometric dependence on the normalized capacitance change of auxetic strain sensor under stretching (a) Dependence of rib thickness of auxetic (b) Dependence of unit width of auxetic.

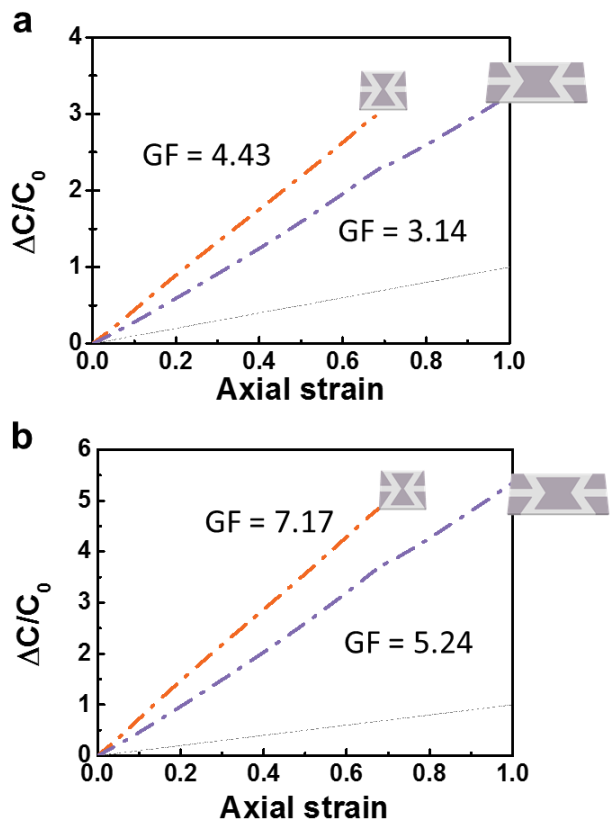

Figure 4.30 Normalized capacitance echange of auxetic composite when (a) Considering both auxetic and filler as a dielectric (b) Considering filler as a dielectric only. From the result, it would be more effective to increase gauge factor covering filler only.

4.6 Summary

In the present study, we developed a soft composite material that can predictively control the elastic properties such as Young's modulus and Poisson's ratio of soft materials by applying auxetic metamaterial. In consideration of both the intrinsic mechanical properties of the material composing the composite and the geometric factor of the auxetic, the developed composite was possible to reach the elastic property which the existing material could not possess. In particular, the greater the difference in the elastic modulus of the material consisting the composite, Poisson's ratio of the composite had a more negative value. Our composite is a full solid body auxetic, and superior to conventional porous auxetic in terms of process feasibility for the soft electronics. Utilizing the anisotropic deformation behavior of composite, we implemented a stretchable and high sensitive capacitive strain sensor. Sensors using conventional isotropic elastomer dielectric have only limited gauge factor to 1. Our auxetic dielectric showed more than 3 times of improvement in sensitivity. Through analytic modeling and numerical analysis, it is expected that it would be possible to to design a sensor with a gauge factor of 7 or more theoretically. Our research ahd a great significance in that we led to the performance improvement of the electronic device through the mechanical design of the material. Our composite has the advantage that it can easily change its mechanical properties, therefore it would be possible to develop a variable fascinating technologies such as multi-directional monitoring sensors via various engineering patterns. It is expected that our composite materials will be a cornerstone to advance several fields of soft electronic devices in the future.

CHAPTER 5

Conclusion

5.1 Summary of results

This study investigated a new strategy of designing flexible electronic by geometric engineering perspective. Auxetic, which was a mechanically reconfigurable metamaterials having negative Poisson's ratio, could be a key structure to control the deformation characteristics in flexible electronics as a platform which could avoid the severe deformation on the active device or predictively control the materials elastic property to enhance electrical performance.

At first, the strain-isolable effect of hierarchical auxetic was investigated under severe and complicated deformation condition. Recent progress in structural engineering for deformable electronics was programmed to be morphing in a specific shape, either stretchable or compressible. In this study, the rotating unit auxetic was found to be 3-dimensionally deformable by replacing the hinge as a flexible joint, and could be deformed in stretching, bending, or twisting. When the hierarchical auxetic underwent severe stretching or crumpling, the mechanical deformation was mainly generated at the hinge, which indicated that the hinges acted as an instable singular point during

deformation. In addition to that, the increase in hierarchy level of auxetic structure could enhance the stretchability and deformability of the whole model. Based on the strain-isolable characteristics of the hierarchical auxetic, extremely deformable batteries were fabricated as a concept of proof. The hierarchical auxetic structure could even be applied to thin film process by modifying the design of hinge.

When the auxetic would embed into soft material, the elastic property of soft material could be predictively controlled depending on the geometry and material's mechanical property of the auxetic structure, and even be able to fabricate the soft materials as a non-porous, flat auxetic material. If the 2-dimensional auxetic was embedded, 3-dimensionally isotropic materials could act as a 2-dimensional auxetic material. When stretched, the thickness of the filling material in the auxetic composite could be decreased more than that of isotropic material due to the volume conservation. This kind of anisotropic deformation property could enhance the electrical performance of capacitive type strain sensor, where the strain sensing mechanism depended on the geometric change under deformation. The gauge factor of the auxetic strain sensor reached to 3.2 where the factor was more than 3 times of the previous capacitive type sensor. The mechanism of improvement was due to the severe thickness decrement of dielectric, rather than the area increment. From the analytical modeling and FEM simulation, the gauge factor was found to be improved more by considering material and geometric perspective. The auxetic sensor could maintain the in-plane auxetic property, therefore had an excellent conformability on the non-zero Gaussian surface, which was another advantage as a wearable electronics.

In conclusion, this thesis could provide a new design concept for modern flexible electronics based on the geometric engineering of mechanically reconfigurable materials.

5.2 Future Work and Suggested Research

Recent issues in stretchable electronics integration focused on the elastic mismatch gap between the substrate and deposited film including elastic modulus and *Poisson*'s ratio. The modern process of electronics was based on the soft elastomeric substrate, while the active film or device layer had still a lot stiffer than the substrate. In mechanical perspective, the modulus gap could induce the local strain concentration at the heterogeneous interface between film and substrate, and the difference in Poisson's ratio could induce surface instability of film such as buckling induced delamination. When the gap would becoming larger, it is more vulnerable to mechanically fail at the heterogeneous interface. From the research of chapter 4, the equivalent modulus and *Poisson*'s ratio of targeted soft material substrate could be predictively be designed by the auxetic composite. By tuning the elastic property of soft substrate material, it would be expected to enhance the mechanical stability of stretchable electronics.

References

[1] Larson C, Peele B, Li S, Robinson S, Totaro M, Beccai L, et al. Highly stretchable electroluminescent skin for optical signaling and tactile sensing. Science 2016;351:1071-4.

[2] Shian S, Bertoldi K, Clarke DR. Dielectric Elastomer Based "Grippers" for Soft Robotics. Advanced materials 2015;27:6814-9.

[3] Gao W, Emaminejad S, Nyein HY, Challa S, Chen K, Peck A, et al. Fully integrated wearable sensor arrays for multiplexed in situ perspiration analysis. Nature 2016;529:509-14.

[4] Jang KI, Chung HU, Xu S, Lee CH, Luan H, Jeong J, et al. Soft network composite materials with deterministic and bio-inspired designs. Nature communications 2015;6:6566.

[5] Kim BJ, Cho Y, Jung MS, Shin HA, Moon MW, Han HN, et al. Fatigue-free, electrically reliable copper electrode with nanohole array. Small 2012;8:3300-6.

[6] Jung MS, Seo JH, Moon MW, Choi JW, Joo YC, Choi IS. A Bendable Li-Ion Battery with a Nano-Hairy Electrode: Direct Integration Scheme on the Polymer Substrate. Adv Energy Mater 2015;5.

[7] Xu S, Zhang Y, Cho J, Lee J, Huang X, Jia L, et al. Stretchable batteries with self-similar serpentine interconnects and integrated wireless recharging systems. Nature communications 2013;4:1543.

[8] van der Sluis O, Hsu YY, Timmermans PHM, Gonzalez M, Hoefnagels JPM. Stretching-induced interconnect delamination in stretchable electronic circuits. J Phys D Appl Phys 2011;44.

[9] Zhang YH, Yan Z, Nan KW, Xiao DQ, Liu YH, Luan HW, et al. A mechanically driven form of Kirigami as a route to 3D mesostructures in micro/nanomembranes. Proceedings of the National Academy of Sciences of the United States of America 2015;112:11757-64.

[10] Boatti E, Vasios N, Bertoldi K. Origami Metamaterials for Tunable Thermal Expansion. Advanced materials 2017;29.

[11] Silverberg JL, Evans AA, McLeod L, Hayward RC, Hull T, Santangelo CD, et al. Using origami design principles to fold reprogrammable mechanical metamaterials. Science 2014;345:647-50.

[12] Wu G, Cho Y, Choi IS, Ge D, Li J, Han HN, et al. Directing the deformation paths of soft metamaterials with prescribed asymmetric units. Advanced materials 2015;27:2747-52.

[13] Evans KE, Alderson A. Auxetic materials: Functional materials and structures from lateral thinking! Advanced materials 2000;12:617-+.

[14] Konakovic M, Crane K, Deng BL, Bouaziz S, Piker D, Pauly M. Beyond Developable: Computational Design and Fabrication with Auxetic Materials. Acm T Graphic 2016;35.

[15] Cho Y, Shin JH, Costa A, Kim TA, Kunin V, Li J, et al. Engineering the shape and structure of materials by fractal cut. Proceedings of the National Academy of Sciences of the United States of America 2014;111:17390-5.

[16] Ogden RW. Nonlinear Elastic Deformations. Dover.

[17] Elipe JCA, Lantada AD. Comparative study of auxetic geometries by means of computer-aided design and engineering. Smart Mater Struct 2012;21.

[18] Ken E. Evans AA, Frances R. Christian. Auxetic Two-dimensional Polymer Networks. An example of tailoring geometry for specific mechanical properties. J Chem

Soc, Faraday Trans 1995;91:2671-80.

[19] Tang Y, Lin G, Han L, Qiu S, Yang S, Yin J. Design of Hierarchically Cut Hinges for Highly Stretchable and Reconfigurable Metamaterials with Enhanced Strength. Advanced materials 2015;27:7181-90.

[20] Kunin V, Yang S, Cho Y, Deymier P, Srolovitz DJ. Static and dynamic elastic properties of fractal-cut materials. Extreme Mech Lett 2016;6:103-14.

[21] Grima JN, Mizzi L, Azzopardi KM, Gatt R. Auxetic Perforated Mechanical Metamaterials with Randomly Oriented Cuts. Advanced materials 2016;28:385-9.

[22] Gatt R, Mizzi L, Azzopardi JI, Azzopardi KM, Attard D, Casha A, et al. Hierarchical auxetic mechanical metamaterials. Scientific reports 2015;5:8395.

[23] Narain R, Pfaff T, O'Brien JF. Folding and Crumpling Adaptive Sheets. Acm T Graphic 2013;32.

[24] Silverberg JL. Origami structures with a critical transition to bistability arising from hidden degrees of freedom. Nature materials 2015;14.

[25] Song Z, Ma T, Tang R, Cheng Q, Wang X, Krishnaraju D, et al. Origami lithium-ion batteries. Nature communications 2014;5:3140.

[26] Song Z, Wang X, Lv C, An Y, Liang M, Ma T, et al. Kirigami-based stretchable lithium-ion batteries. Scientific reports 2015;5:10988.

[27] Lamoureux A, Lee K, Shlian M, Forrest SR, Shtein M. Dynamic kirigami structures for integrated solar tracking. Nature communications 2015;6:8092.

[28] Wehner M, Truby RL, Fitzgerald DJ, Mosadegh B, Whitesides GM, Lewis JA, et al. An integrated design and fabrication strategy for entirely soft, autonomous robots. Nature 2016;536:451-5.

[29] Li CH, Wang C, Keplinger C, Zuo JL, Jin L, Sun Y, et al. A highly stretchable autonomous self-healing elastomer. Nat Chem 2016;8:619-25.

[30] Lee YY, Kang HY, Gwon SH, Choi GM, Lim SM, Sun JY, et al. A Strain-Insensitive Stretchable Electronic Conductor: PEDOT:PSS/Acrylamide Organogels. Advanced materials 2016;28:1636-43.

[31] Kim CC, Lee HH, Oh KH, Sun JY. Highly stretchable, transparent ionic touch panel. Science 2016;353:682-7.

[32] Lee JW, Xu RX, Lee S, Jang KI, Yang YC, Banks A, et al. Soft, thin skin-mounted power management systems and their use in wireless thermography. Proceedings of the National Academy of Sciences of the United States of America 2016;113:6131-6.

[33] Li S, Zhao HC, Shepherd RF. Flexible and stretchable sensors for fluidic elastomer actuated soft robots. Mrs Bull 2017;42:138-42.

[34] Lee YY, Lee JH, Cho JY, Kim NR, Nam DH, Choi IS, et al. Stretching-Induced Growth of PEDOT-Rich Cores: A New Mechanism for Strain-Dependent Resistivity Change in PEDOT:PSS Films. Adv Funct Mater 2013;23:4020-7.

[35] Javid F, Smith-Roberge E, Innes MC, Shanian A, Weaver JC, Bertoldi K. Dimpled elastic sheets: a new class of non-porous negative Poisson's ratio materials. Scientific reports 2015;5:18373.

[36] Gatt R, Vella Wood M, Gatt A, Zarb F, Formosa C, Azzopardi KM, et al. Negative Poisson's ratios in tendons: An unexpected mechanical response. Acta biomaterialia 2015;24:201-8.

[37] Cai L, Song L, Luan P, Zhang Q, Zhang N, Gao Q, et al. Super-stretchable, transparent carbon nanotube-based capacitive strain sensors for human motion detection. Scientific reports 2013;3:3048.

[38] Cohen DJ, Mitra D, Peterson K, Maharbiz MM. A highly elastic, capacitive strain gauge based on percolating nanotube networks. Nano letters 2012;12:1821-5.

[1] Kim Y, Zhu J, Yeom B, Di Prima M, Su X, Kim JG, et al. Stretchable nanoparticle

conductors with self-organized conductive pathways. Nature 2013;500:59-63.

[2] Kim CC, Lee HH, Oh KH, Sun JY. Highly stretchable, transparent ionic touch panel. Science 2016;353:682-7.

[3] Sun JY, Keplinger C, Whitesides GM, Suo Z. Ionic skin. Advanced materials 2014;26:7608-14.

[4] Kim MG, Alrowais H, Pavlidis S, Brand O. Size-Scalable and High-Density Liquid-Metal-Based Soft Electronic Passive Components and Circuits Using Soft Lithography. Adv Funct Mater 2017;27.

[5] Larson C, Peele B, Li S, Robinson S, Totaro M, Beccai L, et al. Highly stretchable electroluminescent skin for optical signaling and tactile sensing. Science 2016;351:1071-4.

[6] Shian S, Bertoldi K, Clarke DR. Dielectric Elastomer Based "Grippers" for Soft Robotics. Advanced materials 2015;27:6814-9.

[7] Gao W, Emaminejad S, Nyein HY, Challa S, Chen K, Peck A, et al. Fully integrated wearable sensor arrays for multiplexed in situ perspiration analysis. Nature 2016;529:509-14.

[8] Jang KI, Chung HU, Xu S, Lee CH, Luan H, Jeong J, et al. Soft network composite materials with deterministic and bio-inspired designs. Nature communications 2015;6:6566.

[9] Kim BJ, Cho Y, Jung MS, Shin HA, Moon MW, Han HN, et al. Fatigue-free, electrically reliable copper electrode with nanohole array. Small 2012;8:3300-6.

[10] Jung MS, Seo JH, Moon MW, Choi JW, Joo YC, Choi IS. A Bendable Li-Ion Battery with a Nano-Hairy Electrode: Direct Integration Scheme on the Polymer Substrate. Adv Energy Mater 2015;5.

[11] Xu S, Zhang Y, Cho J, Lee J, Huang X, Jia L, et al. Stretchable batteries with self-

similar serpentine interconnects and integrated wireless recharging systems. Nature communications 2013;4:1543.

[12] van der Sluis O, Hsu YY, Timmermans PHM, Gonzalez M, Hoefnagels JPM. Stretching-induced interconnect delamination in stretchable electronic circuits. J Phys D Appl Phys 2011;44.

[13] Zhang YH, Yan Z, Nan KW, Xiao DQ, Liu YH, Luan HW, et al. A mechanically driven form of Kirigami as a route to 3D mesostructures in micro/nanomembranes. Proceedings of the National Academy of Sciences of the United States of America 2015;112:11757-64.

[14] Boatti E, Vasios N, Bertoldi K. Origami Metamaterials for Tunable Thermal Expansion. Advanced materials 2017;29.

[15] Silverberg JL, Evans AA, McLeod L, Hayward RC, Hull T, Santangelo CD, et al. Using origami design principles to fold reprogrammable mechanical metamaterials. Science 2014;345:647-50.

[16] Wu G, Cho Y, Choi IS, Ge D, Li J, Han HN, et al. Directing the deformation paths of soft metamaterials with prescribed asymmetric units. Advanced materials 2015;27:2747-52.

[17] Evans KE, Alderson A. Auxetic materials: Functional materials and structures from lateral thinking! Advanced materials 2000;12:617-+.

[18] Konakovic M, Crane K, Deng BL, Bouaziz S, Piker D, Pauly M. Beyond Developable: Computational Design and Fabrication with Auxetic Materials. Acm T Graphic 2016;35.

[19] Cho Y, Shin JH, Costa A, Kim TA, Kunin V, Li J, et al. Engineering the shape and structure of materials by fractal cut. Proceedings of the National Academy of Sciences of the United States of America 2014;111:17390-5.

[20] Ogden RW. Nonlinear Elastic Deformations. Dover.

[21] Elipe JCA, Lantada AD. Comparative study of auxetic geometries by means of computer-aided design and engineering. Smart Mater Struct 2012;21.

[22] Ken E. Evans AA, Frances R. Christian. Auxetic Two-dimensional Polymer Networks. An example of tailoring geometry for specific mechanical properties. J Chem Soc, Faraday Trans 1995;91:2671-80.

[23] Tang Y, Lin G, Han L, Qiu S, Yang S, Yin J. Design of Hierarchically Cut Hinges for Highly Stretchable and Reconfigurable Metamaterials with Enhanced Strength. Advanced materials 2015;27:7181-90.

[24] Kunin V, Yang S, Cho Y, Deymier P, Srolovitz DJ. Static and dynamic elastic properties of fractal-cut materials. Extreme Mech Lett 2016;6:103-14.

[25] Grima JN, Mizzi L, Azzopardi KM, Gatt R. Auxetic Perforated Mechanical Metamaterials with Randomly Oriented Cuts. Advanced materials 2016;28:385-9.

[26] Gatt R, Mizzi L, Azzopardi JI, Azzopardi KM, Attard D, Casha A, et al. Hierarchical auxetic mechanical metamaterials. Scientific reports 2015;5:8395.

[27] Narain R, Pfaff T, O'Brien JF. Folding and Crumpling Adaptive Sheets. Acm T Graphic 2013;32.

[28] Silverberg JL. Origami structures with a critical transition to bistability arising from hidden degrees of freedom. Nature materials 2015;14.

[29] Song Z, Ma T, Tang R, Cheng Q, Wang X, Krishnaraju D, et al. Origami lithium-ion batteries. Nature communications 2014;5:3140.

[30] Song Z, Wang X, Lv C, An Y, Liang M, Ma T, et al. Kirigami-based stretchable lithium-ion batteries. Scientific reports 2015;5:10988.

[31] Lamoureux A, Lee K, Shlian M, Forrest SR, Shtein M. Dynamic kirigami structures for integrated solar tracking. Nature communications 2015;6:8092.

[32] Wehner M, Truby RL, Fitzgerald DJ, Mosadegh B, Whitesides GM, Lewis JA, et al. An integrated design and fabrication strategy for entirely soft, autonomous robots. Nature 2016;536:451-5.

[33] Li CH, Wang C, Keplinger C, Zuo JL, Jin L, Sun Y, et al. A highly stretchable autonomous self-healing elastomer. Nat Chem 2016;8:619-25.

[34] Lee YY, Kang HY, Gwon SH, Choi GM, Lim SM, Sun JY, et al. A Strain-Insensitive Stretchable Electronic Conductor: PEDOT:PSS/Acrylamide Organogels. Advanced materials 2016;28:1636-43.

[35] Lee JW, Xu RX, Lee S, Jang KI, Yang YC, Banks A, et al. Soft, thin skin-mounted power management systems and their use in wireless thermography. Proceedings of the National Academy of Sciences of the United States of America 2016;113:6131-6.

[36] Li S, Zhao HC, Shepherd RF. Flexible and stretchable sensors for fluidic elastomer actuated soft robots. Mrs Bull 2017;42:138-42.

[37] Lee YY, Lee JH, Cho JY, Kim NR, Nam DH, Choi IS, et al. Stretching-Induced Growth of PEDOT-Rich Cores: A New Mechanism for Strain-Dependent Resistivity Change in PEDOT:PSS Films. Adv Funct Mater 2013;23:4020-7.

[38] Javid F, Smith-Roberge E, Innes MC, Shanian A, Weaver JC, Bertoldi K. Dimpled elastic sheets: a new class of non-porous negative Poisson's ratio materials. Scientific reports 2015;5:18373.

[39] Gatt R, Vella Wood M, Gatt A, Zarb F, Formosa C, Azzopardi KM, et al. Negative Poisson's ratios in tendons: An unexpected mechanical response. Acta biomaterialia 2015;24:201-8.

[40] Cai L, Song L, Luan P, Zhang Q, Zhang N, Gao Q, et al. Super-stretchable, transparent carbon nanotube-based capacitive strain sensors for human motion detection. Scientific reports 2013;3:3048.

[41] Cohen DJ, Mitra D, Peterson K, Maharbiz MM. A highly elastic, capacitive strain gauge based on percolating nanotube networks. Nano letters 2012;12:1821-5.

요약(국문초록)

사용자의 편의성을 위한 유연소자의 발전이 진행됨에 따라, 유연소자를 구성하는 소재 뿐 아니라 유연성 향상 및 특정한 형태로 변형될 수 있는 구조 개발에 대한 연구가 활발하게 진행되고 있다. 구조 혁신을 통한 기계적 특성 조절은 기존의 소재적 한계를 벗어나는 새로운 물성을 부여할 수 있고, 예측 가능하게 설계하기 쉽다는 장점이 있다. 이러한 특징에 기인하여, 외부의 물리적 자극에 반응하여 동작할 수 있는 가변 구조 재료에 대한 관심이 점차 높아지고 있다. 기계적 가변 재료 중 하나인 옥세틱(Auxetic)은 음의 푸아송 비를 가지므로 팽창률이 우수하고 비가우시안 평면에서도 우수한 접착형상을 유지할 수 있어 차세대 유연소자용 구조재료로써 주목받고 있다. 본 연구에서는, 다양한 2 차원 옥세틱 구조의 기하학적 요소 디자인을 통해 유연소자의 기계적·전기적 성능을 향상시키는 연구에 대해 진행하였으며, 이를 통해 유연소자 용 구조재료의 새로운 패러다임을 제시하고자 한다.

첫째로, 자가닮음 계층 구조를 갖는 회전 유닛 옥세틱 구조를 이용하여 이를 전방향으로 대변형이 가능한 유연소자 용 플랫폼으로 제안하였다. 유한요소해석을 통해, 계층구조 회전 유닛 옥세틱이 인장 뿐 아니라 구김 등의 복잡한 변형을 거치더라도 각 유닛을 연결하는 힌지 부분에서만 변형을 집중시킬 수 있다는 것을 증명하였으며, 이러한 변형 특징에 착안하여 전방향으로 대변형이 가능한 배터리를 개발하였다. 힌지가 기계적 안정성이 우수한 탄성체로 구성될 경우, 기존의 2 차원 auxetic 관점에서는 생각하지 못했던 3 차원적인 변형이 가능하며, 힌지의 변형 자유도가 무한대로 늘어날 수 있다. 또한, 계층 구조의 레벨이 증가함에 따라 동일 수준의 변형에도 힌지에 집중되는 스트레인이 완화되어

기계적 안정성이 향상되며, 전체 구조의 신축성이 향상되고 쉽게 구겨질 수 있다는 것을 확인하였다. 커팅 공정을 통해 얇은 플라스틱 기판에서도 동일한 계층구조 옥세틱을 디자인할 수 있으며, 이 경우 날카로운 컷 구조로 인하여 쉽게 찢어짐이 발생할 수 있다. 이를 방지하기 위해 균열의 진행을 가로막는 힌지 디자인을 개발함으로써 얇은 시트에서도 동일한 옥세틱 구조를 적용할 수 있다는 가능성을 확인할 수 있었다.

둘째로, 2 차원 요각 구조 옥세틱을 소프트 재료의 복합 골자로 적용함으로써 탄성 계수와 푸아송 비가 예측 설계할 수 있는 옥세틱 복합체를 개발하였다. 또한, 유한요소해석을 통해 복합체 골자로 사용한 요각 구조의 기하학적 요소와, 복합체 소재 간 탄성 계수의 차이에 따른 복합체의 탄성 물성 예측 가능하게 설계할 수 있다는 것을 확인하였다. 이러한 옥세틱 복합체는 차원의 요각 구조의 영향으로 비등방성 변형 거동을 갖게 되는데, 인장에 대해 평면 내에서는 음의 푸아송 비 거동을, 그리고 두께 방향으로는 양의 푸아송 비를 가지게 된다. 특히, 복합체를 이루는 모상은 부피를 보존하기 위해 인장에 따른 수직방향 두께가 등방성 소재보다 더욱 빠르게 감소하게 된다. 이러한 비등방성 거동 특징을 이용하여, 복합체를 정전용량 성 고신축성 (~50 %) 스트레인 센서의 유전체로 사용하여 성능을 향상시키는 연구를 진행하였다. 스트레인 대비 정전용량 변화율을 의미하는 게이지 팩터(Gauge factor)는 통상의 스트레인 센서가 소재에 관계없이 항상 1 로 고정되는 한계가 존재하였으나, 옥세틱 복합체를 이용하여 기존 정전용량 성 스트레인 센서의 한계를 극복하였다. 뿐만 아니라, 복합체가 평면 상으로 음의 푸아송 비 거동을 보이기 때문에 팔꿈치나 무릎 등의 양의 가우시안 곡률면에도 우수한 접착면을 유지함으로써 웨어러블 센서 용 기하구조 디자인의 새로운 방향을 제시하였다.

본 연구는 옥세틱이라는 기계적 메타재료를 필요에 맞게 맞춤 설계하여 현재 개발되고 있는 다양한 유연 소자의 기계적, 전기적 성능을 향상시킴으로써 유연 소자용 구조 재료로서의 새로운 방향을 제시할 수 있을 것으로 기대된다.

표제어: Auxetic, Geometric engineering, Reconfigurable materials, Flexible electronics, Mechanical metamaterial

학 번: 2011-20659